The impact of future sea-level rise on the global tides

M.D. Pickering[a,*], K.J. Horsburgh[b], J.R. Blundell[a], J.J.-M. Hirschi[c], R.J. Nicholls[d], M. Verlaan[e,f], N.C. Wells[a]

[a] Ocean and Earth Science, National Oceanography Centre, University of Southampton Waterfront Campus, European Way, Southampton SO14 3ZH, United Kingdom
[b] National Oceanography Centre, Joseph Proudman Building, Brownlow Street, Liverpool L3 5DA, United Kingdom
[c] National Oceanography Centre, University of Southampton Waterfront Campus, European Way, Southampton SO14 3ZH, United Kingdom
[d] Engineering and the Environment, University of Southampton, Highfield, Southampton SO17 1BJ, United Kingdom
[e] Deltares, Rotterdamseweg 185, 2629 HD Delft, The Netherlands
[f] Delft University of Technology, Mekelweg 4, 2628 CD Delft, The Netherlands

A R T I C L E   I N F O

A B S T R A C T

Tides are a key component in coastal extreme water levels. Possible changes in the tides caused by mean sea-level rise (SLR) are therefore of importance in the analysis of coastal flooding, as well as many other applications. We investigate the effect of future SLR on the tides globally using a fully global forward tidal model: OTISmpi. Statistical comparisons of the modelled and observed tidal solutions demonstrate the skill of the refined model setup with no reliance on data assimilation. We simulate the response of the four primary tidal constituents to various SLR scenarios. Particular attention is paid to future changes at the largest 136 coastal cities, where changes in water level would have the greatest impact.

Spatially uniform SLR scenarios ranging from 0.5 to 10 m with fixed coastlines show that the tidal amplitudes in shelf seas globally respond strongly to SLR with spatially coherent areas of increase and decrease. Changes in the M2 and S2 constituents occur globally in most shelf seas, whereas changes in K1 and O1 are confined to Asian shelves. With higher SLR tidal changes are often not proportional to the SLR imposed and larger portions of mean high water (MHW) changes are above proportional. Changes in MHW exceed ± 10% of the SLR at ~10% of coastal cities. SLR scenarios allowing for coastal recession tend increasingly to result in a reduction in tidal range. The fact that the fixed and recession shoreline scenarios result mainly in changes of opposing sign is explained by the effect of the perturbations on the natural period of oscillation of the basin. Our results suggest that coastal management strategies could influence the sign of the tidal amplitude change. The effect of a spatially varying SLR, in this case fingerprints of the initial elastic response to ice mass loss, modestly alters the tidal response with the largest differences at high latitudes.

1. Introduction

Sea-level rise (SLR) has been observed from tide gauges over the 20th century at an average rate of 1.7 mm/yr (Church and White, 2011) and by altimetry over the period from 1993 to 2016 at average rate of 3.3 mm/y (Nerem and NCAR, 2016). The most recent Intergovernmental Panel on Climate Change Fifth Assessment Report (IPCC AR5) projections for 2100 SLR range from the lower end (5%) of the likely (66–100%) range for RCP2.6[1] at 0.28 m to the higher end (95%) of the likely range for RCP8.5 at 0.98 m (Church et al., 2014). In addition to these medium confidence process based model projections

there are also low confidence semi-empirical models which give projections for SLR by 2081–2100 with median values from 0.4 m for RCP2.6 (Jevrejeva et al., 2012) to 1.2 m for RCP8.5 (Grinsted et al., 2010; Jevrejeva et al., 2012). Other methodologies suggest upper limits of 2100 SLR from 1.15 m (Katsman et al., 2011) to 2.25 m (Sriver et al., 2012). AR5 states it is virtually certain (99–100%) that SLR will continue beyond 2100 and with a low confidence estimates that SLR of 1–3 m for each degree Celsius of warming will occur assuming the warming is sustained for several millennia (Church et al., 2014).

In this paper, we consider the effect of future SLR on a component of extreme water levels which has received less attention- the global

---

* Corresponding author.
E-mail addresses: mdp053@gmail.com (M.D. Pickering), kevinh@noc.ac.uk (K.J. Horsburgh), jeff@noc.soton.ac.uk (J.R. Blundell),
joel.hirschi@noc.soton.ac.uk (J.J.-M. Hirschi), R.J.Nicholls@soton.ac.uk (R.J. Nicholls), Martin.Verlaan@deltares.nl (M. Verlaan), N.C.Wells@soton.ac.uk (N.C. Wells).

[1] The IPCC AR5 uses Representative Concentration Pathways (RCPs) to explore the potential range of future emissions of important gases and aerosols. The value following RCP indicates the peak or stabilization radiative forcing in (W/m2) for the year 2100; from the lowest RCP 2.6 to the highest RCP 8.5.

tides. Secular trends in tidal characteristics (e.g. constituent phase and amplitude) are observed in many tide gauge records (Woodworth et al., 1991; Flick et al., 2003; Hollebrandse, 2005; Dillingh, 2006; Pouvreau et al., 2006; Ray, 2006, 2009; Jay, 2009; Haigh et al., 2010a; Woodworth, 2010; Müller, 2011; Mudersbach et al., 2013). Efforts have been made to relate these observed trends in the tides to modelled changes associated with observed SLR in global tidal models (Müller et al., 2011). Difficulties can occur as observed tides will vary due to morphological changes, dredging, harbour creation, land reclamation and tectonic effects as well as sea-level variability. Compounding this, the distribution of tide gauges is biased towards port locations where anthropogenic factors are most influential.

Given the uncertainties in the future SLR patterns (Milne et al., 2009; Slangen et al., 2014) and the fact that ~70% of global coastlines are projected to experience a sea-level change within 20% of the global mean (Church et al., 2014), we initially investigate the response of tides to idealised uniform global SLR scenarios. We then explore two predicted geometries of non-uniform SL change due to continuing ice mass variations of Greenland or Antarctica, as well as a combination of the two, using fingerprints from Mitrovica et al. (2001). These fingerprints include the static initial elastic response (IER) to present day ice mass loss and the gravitational effects but not the longer-term viscous flow effect or the continuing GIA response to melting of late Pleistocene ice.

Other modelling studies have tended to focus on changes in the tides associated with the large (~125 m) Last Glacial Maximum to present or Holocene (~35 m) SLR (Austin, 1991; Gerritsen and Berentsen, 1998; Egbert et al., 2004; Uehara et al., 2006; Griffiths and Peltier, 2009; Green, 2010). A selection of the methodologies and results of previous studies of future SLR and European shelf tides are reviewed in Table 4 of Pickering et al. (2012). This study found substantially larger changes in the dominant semidiurnal tidal constituents of the European Shelf than previous studies (e.g. Lowe et al., 2001) with amplitudes responding non-uniformly with both increases and decreases across the shelf. Comparison with previous studies highlighted the importance of a high resolution model, a complete spatial rather than single point analysis, and a relatively large SLR scenario when identifying tidal changes with future SLR. Subsequent regional studies have also shown changes in tides with SLR in other areas such as the Bay of Fundy, USA (Greenberg et al., 2012; Pelling and Green, 2013), the Bohai Sea, China (Pelling et al., 2013b) and the Gulf of Mexico (Passeri et al., 2016). Regional modelling studies of changing tides are subject to issues of model intercomparability and assumptions regarding tidal characteristics around the model's open boundary. The results of Pickering et al. (2012) motivated us to investigate the effect of future SLR on the global tides using a single, global domain.

We selected the Oregon State University OTISmpi model owing to its thorough and published validation (Egbert et al., 2004), global domain with no open boundaries, inclusion of an internal wave dissipation parameterisation (Zaron and Egbert, 2006), self-consistent iterative scheme for self-attraction and loading (SAL), and lack of requirement for any data assimilation. Global tidal models (and compute power) have progressed a long way since the early work of Schwiderski (1980). This has been made possible by improved observations of the global tides from satellite altimetry which complemented those from the existing tide gauge network (Provost, 2001), as well as enabling estimates of global tidal dissipation through friction at the bed and internal wave drag (Egbert and Ray, 2001).

The changes to tidal characteristics caused by future SLR presented in this paper have important long-term global implications. Examples include coastal flood risk and management, tidal renewable energy, sediment transport and dredging, tidal mixing fronts and intertidal ecology (Pickering, 2014).

The objectives of this study are: (1) to assess the effect of uniform future SLR on the four primary semidiurnal and diurnal tidal con-

stituents; (2) to assess the importance of coastal recession with SLR (which we approximate by moving the model coastline and allowing changes to the number of wet cells in the model domain) rather than assuming a fixed coastline; (3) to evaluate the proportionality of the tidal changes to the SLR imposed; and (4) to assess the effect on tidal changes of including non-uniform SLR associated with IER scenarios. We present global results, but also focus on regional enlargements as well as analysis of 136 coastal cities with populations over 1 million (in 2005) in order to draw attention to localised impacts. The mean high water metric is used throughout as it incorporates the combined effect of changes in all four tidal constituents; also it can be used in calculation of extreme water level return periods used in coastal flood defence design and by coastal engineers (Pugh and Vassie, 1980; Caires et al., 2007). Maximum tidal range over the 15 day reconstruction (see Section 2.3) is also evaluated as it is a relevant metric for renewable energy extraction.

The paper is structured as follows: Section 2 gives specifics of the model setup and additional validation, the data analysis and inherent assumptions; Section 3 presents the results of the study relating to the objectives above; before Section 4 discusses the significance of the results and their implications, Section 5 ends with the conclusions.

2. Method

2.1. Refinement of model setup and additional validation

OTISmpi solves the non-linear shallow water equations on a C-grid using a finite differences time stepping method. Details of the model and its validation can be found in Egbert et al. (2004) and references therein. Specific choices regarding our setup of the model are detailed in this section. Egbert et al. (2004) present results for a nearly global tidal model with an open boundary in the high Arctic; here we employ the newer fully global North Pole in Greenland (NPG) version which gives similar results (Egbert et al., 2004). The absence of any open boundary condition or data assimilation in this prognostic model leaves the model free to evolve to a possibly different future tidal equilibrium (in response to the sea-level rise (SLR) perturbation).

The code was ported to the local cluster and verified using benchmark 1/8th degree, 2 constituent OTISmpi NPG solutions provided by Oregon State University. The M2 and K1 tidal amplitudes were accurately replicated with a maximum grid point amplitude difference of 0.18 mm - at least two orders of magnitude smaller than the tidal amplitudes of interest.

To validate the model for present day tidal solutions we make statistical comparison with the FES2004 tidal atlas solutions (Lyard et al., 2006). The FES2004 solutions were regarded as the best estimates of the global tides available, and are generated using a hydrodynamic model assimilating large datasets of tide gauge and altimetric observations. We use the Root Mean Square Error (RMSE)

$$RMSE = \sqrt{\frac{\sum_{i=1}^{n} [(Hm_i - Ho_i)^2] a_i}{\sum_{i=1}^{n} a_i}} \tag{1}$$

where Hm_i and Ho_i are tidal constituent amplitudes at grid point i for the OTISmpi model solution and FES2004 observation respectively and a_i is the surface area of the grid cell at point i and the Vector Difference (VD)

$$VD = \sqrt{\frac{\sum_{i=1}^{n} [(Rm_i - Ro_i)^2 + (Im_i - Io_i)^2] a_i}{\sum_{i=1}^{n} a_i}} \tag{2}$$

where Rm_i and Ro_i are the real parts at grid point i modelled and observed respectively; Im_i and Io_i are the imaginary parts at grid point i, modelled and observed respectively. The real and imaginary parts are defined as:

Table 1

Root Mean Square Error (RMSE) and Vector Difference (VD) statistical validation (see Eqs. (1) and (2) for formulations) against the FES2004 tidal atlas solutions for different physical model setups and constituents. Global statistics are also separated into Shelf (< 200 m) and Deep Water (> 200 m) parts. Details of differences between Default and Refined model setups can be found in Section 2.1. Statistics for the Control (also referred to as present day) setup are listed as Refined (SAL it.4).

Model Setup	Constituent	RMSE (cm)			VD (cm)		
		Global	Shelf	Deep Water	Global	Shelf	Deep Water
Default (SAL it.0)	M2	12.6	28.8	10.7	21.6	45.9	18.9
Refined (SAL it.0)	M2	15.7	28.8	14.4	20.5	43.5	17.9
Refined (SAL it.4)	M2	10.1	21.2	8.9	13.9	30.4	12.0
Refined (SAL it.4)	S2	5.0	10.8	4.3	7.1	14.8	6.3
Refined (SAL it.4)	K1	2.7	7.1	2.2	4.2	12.2	2.9
Refined (SAL it.4)	O1	2.7	5.8	2.4	3.4	8.4	2.8

$Rm_i = Hm_i \cos(Gm_i)$ or $Ro_i = Ho_i \cos(Go_i)$ and
$Im_i = Hm_i \sin(Gm_i)$ or $Io_i = Ho_i \sin(Go_i)$

where Gm_i and Go_i are modelled and observed phases respectively. The RMSE gives an indication of the model skill at calculating tidal amplitudes whereas the VD is a simultaneous measure of both phase and amplitude error. Global values for these statistics are given as well as the values for shelf and deep water parts; the shelf edge is defined as 200 m depth. These statistics provide a quantitative means of assessing whether changes to the model setup have improved its skill at calculating present day tides.

After benchmarking some adjustments were made to give the Default model setup in Table 1. Firstly we use Version 2 (2008) of the GEBCO One Minute Grid topography (http://www.gebco.net) rather than Version 1. Version 2 contains a number of improvements which resulted in small reductions (Global 0.1 cm; Shelf 0.4 cm) in the RMSE values for M2. Secondly the 10.4 day run including a 3.5 day harmonic analysis was extended to a 50 day run including a 10 day harmonic analysis. Run lengths up to 60 days were explored however validation statistics converged (to the nearest 0.1 cm) after 50 days. This study uses a model resolution of 1/8×1/8 degree (~14×14 km at its coarsest equatorial resolution). Egbert et al. (2004) show in their validation the M2 RMSE has largely converged at 1/8 degree with only very slight improvements at a 1/12 degree. The substantially larger computational requirement of using 1/12 degree resolution did not justify the marginal accuracy increase.

This Default model was then refined to maximise accuracy of the present day tide and to ensure the setup was appropriate for SLR perturbation experiments. The Refined model runs were forced with, and harmonically analysed for, the dominant M2, S2, K1 and O1 constituents. These constituents have relative coefficients of 1.0 (M2), 0.584 (K1), 0.465 (S2) and 0.415 (O1); the next largest component, P1, was not included having a relative coefficient of only 0.193 (Pugh, 1987). M2 RMSE statistics improved when S2 and O1 were added (Global 0.3 cm; Shelf 1.6 cm); this is most likely due to more representative levels of friction at the bed. The model parallelised well on the 256 cores available however further constituents were not included as they increased runtime approximately linearly. To satisfy the Rayleigh Criterion for the Refined set of constituents (14.77 days for M2-S2 and 13.66 days for O1- K1) a longer harmonic analysis window of 20days was selected.

The Refined model setup also included the Zaron and Egbert (2006) internal tidal drag parameterisation. This yielded a substantial improvement in the M2 RMSE (Global 5.4 cm; Shelf 8.3 cm; Deep water

5.3 cm). This is to be expected given that approximately a third of tidal energy is dissipated through internal wave drag (Egbert and Ray, 2000; Lyard et al., 2006) and its omission would lead to a substantial underestimate of the energy dissipation in the simulations. A scaling factor can be applied to the internal drag parameterisation (Egbert et al., 2004). Although factors greater than 1 gave some global RMSE improvements, the increased energy dissipation was leading to consistent under prediction of shelf tidal amplitudes therefore no scaling factor was applied.

The model setup used the modified iterative self-attraction and loading (SAL) scheme described in Egbert et al. (2004). The Default model setup (SAL iteration 0) M2 RMSE benefited substantially (Global 8.8 cm; Shelf 10.1 cm; Deep water 9.2 cm) from the SAL being initialised with TPXO.5 based tidal solutions, when compared with the Refined model setup initialised with a uniform 10% reduction of the horizontal pressure gradient. This simple uniform correction was chosen to initialise the Refined model setup for two reasons: (1) it was important that the model setup did not rely on any present day observational data, even if indirectly, so that the tidal regime can reach its altered future state with the SLR perturbation; (2) by the fourth SAL iteration the validation statistics were almost identical (< 0.1 cm difference) regardless of the initialisation approach. For each SL scenario the model was run five times with four iterations of the SAL scheme (statistics converged to < 0.07 cm difference). The improvement of the M2 RMSE and VD from SAL iteration 0 to iteration 4 with the Refined model setup can be seen in Table 1.

The bed drag coefficient (Cd) was kept at its default value of 0.003. The drying-rewetting scheme yielded only slight improvements to the validation statistics and given the one third increase in computational requirement it was not included.

The final RMSE and VD values for each of the four constituents used in the results (Refined SAL it. 4) including all the aforementioned model setup choices are given in Table 1. The satisfactorily small differences between the Refined OTISmpi and FES2004 tidal solutions, in addition to the Egbert et al. (2004) validation, give a high degree of confidence in the model's ability to represent the present day tides. The quality of the shelf validation statistics is comparable to operational regional tide-surge models (e.g. Gebraad and Philippart, 1998). Furthermore any residual model errors will exist in both the control and SLR perturbation simulations, and these will cancel out when assessing tidal changes between two model runs. Although smaller relative changes may be valid results, in this investigation we consider amplitude changes ≥5 cm or ≤−5 cm to be significant.

2.2. Inclusion of sea-level rise (SLR)

The selection of SLR scenarios explored are given in Table 2, the coded abbreviations therein are used in the rest of this paper. This

Table 2

Scope of SL scenarios simulated for this investigation giving the abbreviations used in the text. Advance (A) refers to the allowance for the coastline to advance in −2UA scenario. IER refers to initial elastic response (also referred to as non-uniform, NU) SLR scenarios; the ratios refer to the proportions of the average SLR coming from Greenland (G), Western Antarctic (WA) or Both (B) ice sheet melt. In addition to these scenarios a present day sea-level or Control scenario was performed for comparison.

Scenario	SLR (m)					SLF (m)
	+0.5	+1	+2	+5	+10	-2
Uniform Fixed (/Advance)	+0.5UF	+1UF	+2UF	+5UF	+10UF	−2UA
Uniform Recession	+0.5UR	+1UR	+2UR	+5UR	+10UR	
IER 2:0 Fixed			+2NUGF			
IER 0:2 Fixed			+2NUWAF			
IER 1:1 Fixed			+2NUBF			
IER 1:1 Recession			+2NUBR			

section discusses the subtleties of introducing SLR to the model bathymetry in different ways.

The present day bathymetry and land topography from the GEBCO Version 2 dataset (2008) is 1/60th degree resolution. The OTISmpi grid generation routine averages up to 56 GEBCO depth values below mean sea-level (MSL) to give the depth of each model grid cell (1/8th degree resolution). At the coast the model cell is defined as wet when > 40% of the values are below MSL, only the average of the wet values is taken (Egbert et al., 2004). After the ocean mask is defined all land topography is removed. The averaging and threshold approach has limitations along the Dutch coastline where in reality high narrow dykes prevent land areas below MSL from flooding. As a result the Dutch coastline is positioned further inland in the model than in reality. There are very few countries with extensive land areas below MSL near the coast so this is an isolated problem.

In addition to exploring the effect of multiple SLR scenarios on the tide this investigation also assesses the effect of assuming a fixed present day coastline (unrealistic, but a frequent model assumption also sometimes referred to as a vertical wall assumption) compared to allowing coastal recession with SLR. It has been suggested that the coastline SLR assumption has an important effect on the tidal response obtained (Pelling et al., 2013a).

In the fixed coastline uniform SLR scenarios from 0.5 to 10 m the domain remains the same as in the present day simulation (Table 3-Control) and the SLR at all grid points is exactly in line with the intended perturbation. These simpler fixed coastline SLR scenarios are used as a baseline against which further factors such as coastal recession can be compared. The most likely future coastline will be some combination of the two conditions, with hard engineering maintaining an approximation to the present coastline in some locations, such as the 136 cities considered in this paper, and coastal recession being allowed in others.

In the recession scenarios, owing to the 1 m vertical resolution of the GEBCO dataset only SLR scenarios > 1 m give any change to the wet area of the model. For this reason the +0.5UR and +1UR scenarios are largely omitted from this paper's results as they are almost identical to the +0.5UF and +1UF scenarios. The changes to the model domain in the recession cases for the 2 m, 5 m and 10 m SLR are given in Table 3. Considering the proportions of SLR imposed the largest newly wetted area occurs with 2 m SLR, with only ~1.7x and ~2.6x this area newly wetted in the 5 m and 10 m SLR scenarios respectively. The uniform SLR recession scenarios also include a limited number of newly dried cells; these are caused by the routine that masks small lakes as coastal geometry changes. In some coastal cells of the recession scenarios the actual SLR imposed is not in line with the intended SLR perturbation, with SLR less than the scenario value or in exceptional cases sea-level falls (SLF). An explanation of this, and the effect of the 2 m minimum depth, is given in Appendix A2. Over the vast majority of the domain the SLR imposed is as intended.

Early experiments allowing coastal recession with SLR led to extensive ice areas of Antarctica being erroneously flooded. This called into question the accuracy of the GEBCO land/ice topography data in Antarctica. Additionally the portions of the ice anchored to land which would inundate with SLR or floating which would rise with SLR are not given in the dataset. Furthermore for the SLR of this magnitude some of this Antarctic ice would be melting. Recession around the Antarctic coastline is therefore not included by uniformly raising the land/ice topography by 15 m (beyond the highest SLR scenario of 10 m).

Our SLR scenarios also explore a range of non-uniform initial elastic response (IER) scenarios (Table 2), incorporating the SL pattern resulting from crustal rebound an alterations to the gravitational fields as determined with an elastic rebound model (Mitrovica et al., 2001). The IER scenarios presented in this paper all have a global average mean SLR of 2 m with varying proportions of this SLR (2:0, 1:1, 0:2) coming from melt of the two major ice sheets Greenland and Antarctica respectively (see Section 3.4 for details). The three patterns of non-uniform SLR used as perturbations to the bathymetry can be seen in Fig. 5, Supplementary Material (SM)17 and SM18. SLR values at the major cities in each of the IER scenarios are given in Table SM1. In the near field of the region of mass loss SLR is small and in close proximity SLFs result, in the far field however SLR values greater than the average occur. It is noteworthy that with the mass losses occurring near the poles some tropical regions, such as Asia, experience substantial SLR under all three melt scenarios. Table 3 gives the domain changes in each of the four IER scenarios. When a fixed coastline assumption is made only newly dried areas occur due to SLFs in close proximity to the mass loss.

A uniform 2 m SLF scenario is also tested to assess the symmetry of the tidal changes about the present day SL. The domain change under this scenario (Table 3) shows a substantial newly dried area. In scenarios where the coastal city grid cell becomes dry it is impossible to present results, causing null values in the tables.

2.3. Tidal analysis methods

Changes in tidal amplitudes are analysed at the group of 136 global port cities with populations greater than 1 million in 2005 identified in Nicholls et al. (2008) and Hanson et al. (2011). Tidal amplitude changes at these locations will be of particular importance for future coastal flood risk. Nine of these cities are located up estuaries too narrow to be represented on the 1/8th degree model grid. For these locations the nearest representative wet point on the model grid was located. To accurately estimate tidal changes upstream in the estuary a higher resolution model would be required. However, the results for representative model points can be considered as boundary conditions for the mouth of an estuarine model. It is also noted that when including coastal recession with SLR the representative model location may no longer be adjacent to the coastline, instead lying slightly

Table 3

The total number of wet cells in the model domain and their area for the SL scenarios in this investigation. Net changes in wet cell number and area are given and broken down into the newly wetted and newly dried cells. SLR scenarios less than 2 m are not shown as the SLR must be > 1 m to cause any changes to the model domain due to the vertical resolution of the GEBCO topography. The limited number of newly dried cells in the SLR recession scenarios are due to specifics of the masking of small lakes routine as described in Section 2.2.

Scenario	Abbreviation	Wet Cell Number		Ocean Area (km^2)		Newly Wetted		Newly Dried	
		Total	Net Change	Total	Net Change	Cells	Area (km^2)	Cells	Area (km^2)
Control	Control	2736397	N.A.	361614954	N.A.	N.A.	N.A.	N.A.	N.A.
2 m SLR Rec.	+2UR	2745671	9274	362879806	1264852	9283	1265590	9	739
5 m SLR Rec.	+5UR	2752614	16217	363770632	2155678	16231	2156943	14	1265
10 m SLR Rec.	+10UR	2761908	25511	364957948	3342993	25521	3343873	10	880
2 m SLR Fixed IER Green	+2NUGF	2735990	−407	361589965	−24990	0	0	407	24990
2 m SLR Fixed IER W.A.	+2NUWAF	2735845	−552	361584571	−30383	0	0	552	30383
2 m SLR Fixed IER Both	+2NUBF	2736144	−253	361600678	−14277	0	0	253	14277
2 m SLR Rec. IER Both	+2NUBR	2744586	8189	362902024	1287070	8644	1313422	455	26352
2 m SLF Advance.	−2UA	2732440	−3957	361049329	−565625	0	0	3957	565625

(a)　　　　　　　　　　　　　　　　　　　　　　　(b)
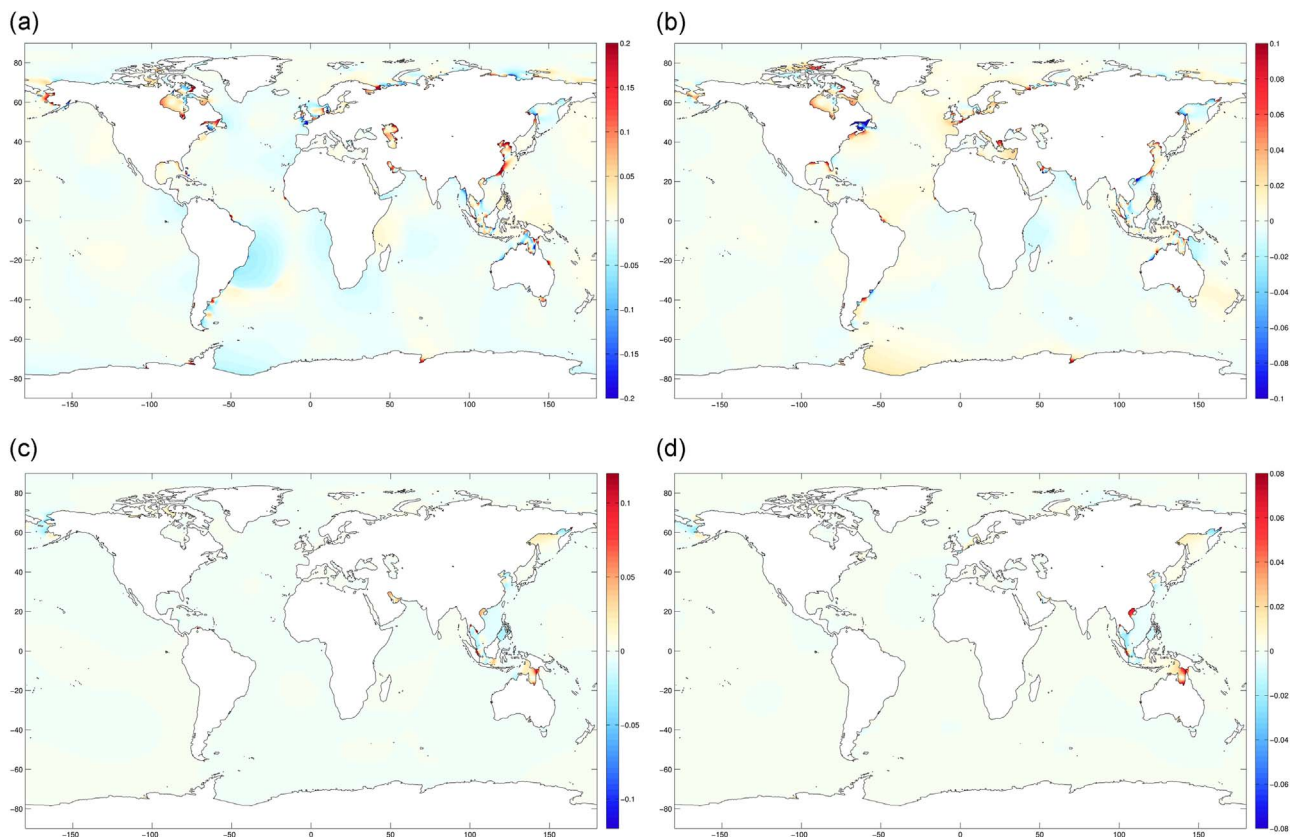
(c)　　　　　　　　　　　　　　　　　　　　　　　(d)

Fig. 1. a-d. Change in amplitude (m) of M2 (a), S2 (b), K1(c) and O1 (d) with 2 m of uniform SLR assuming a fixed present day coastline (+2UF) (increases- red, decreases- blue). Colour scale limits between constituents scaled in proportion to equilibrium tidal amplitudes. For coastal city changes see Table 4.

offshore; to maintain comparability the same point is used however it is recognised that the city itself is likely to have shifted inland in line with the recession.

In order to present manageable tables a sample of 40 of the 136 cities analysed is taken based on different selection criteria explained in the table captions (the full versions of Tables 4, 5, 8 and TSM2 with results for all cities are available in the online SM). For context all city tidal change tables provide the present day population and asset exposure ranking (out of 136, with 1 being the highest) based on the Nicholls et al. (2008) assessment. Future exposure rankings are complex depending on future SLR and storminess, land subsidence, population growth, economic growth, urbanisation and flood defences as well as the potential tidal changes; see Nicholls et al. (2008) and Hallegatte et al. (2013) for details.

In addition to changes in the individual tidal constituents, we also present changes in the mean high water (MHW). This is a useful metric for illustrating the combined effects of the constituent changes as well as an influencing factor in coastal flood risk. Conceptually the mean of the high water values over a 15 day sea surface height (SSH) reconstruction based on four tidal constituents (Eq. (3)) seems straightforward.

$$SSH_i(t) = \sum_c Hm_{ci} \cos(\omega_c t - Gm_{ci})$$

(3)

where SSH at grid point i and time t (in 600 s intervals up to 15 tidal days) is the sum of the four tidal constituents c (M2, S2, K1, O1) with angular frequencies ω_c in radians/s. However when one considers the variation in shape of the tidal signal at all points globally the peaks that should be included as high waters become ambiguous. A substantial methodological development (see Appendix A3) was required in order to obtain a smooth physically plausible MHW (and MLW) field (Fig. SM2).

To complement these mean values the maximum tidal range for the 15 day period was also analysed. This definition of maximum range includes maxima due to both spring tides (semidiurnal regions) and tropical tides (diurnal regions) but not the longer term variations such as equinoctial or nodal tides (Pugh, 2004). These tides are an important part of the tidal cycle for both coastal flooding and renewable energy generation. In Section 3.5, changes in maximum range are analysed for points deemed presently viable for tidal renewable energy. The criteria for viable points is: for tidal barrages a MTR > 5 m, and for tidal stream a water depth 25–100 m with peak current velocities > 2 m/s. For this absolute current velocity times series (U) based on the four constituents for 15 days were computed (Eq. (4)).

$$U_i(t) = \sqrt{\left[\sum_c Hum_{ci} \cos(\omega_c t - Gum_{ci})\right]^2 + \left[\sum_c Hvm_{ci} \cos(\omega_c t - Gvm_{ci})\right]^2}$$

(4)

where U (m/s) at grid point i and time t (in 600 s intervals up to 15 tidal days) is the sum of the four tidal constituents c (M2, S2, K1, O1) for the u component (amplitude (Hum) and phase (Gum)) and the v component (amplitude (Hvm) and phase (Gvm)) of velocity.

Whether the tidal changes at a location are proportional to the SLR imposed is of interest to stakeholders who may wish to interpolate between or extrapolate from tidal changes for particular SLR scenarios. Using a range of uniform SLR scenarios (Table 2) we assess proportionality using the normalised ratio (with respect to the SLR scenarios) of the change for any tidal property (M2, S2, K1, O1, MHW, Maximum Range) for the SLR scenario to the change in that property with 0.5 m SLR. Allowing a 10% range about a ratio of unity we define a proportional response as, for example, a MHW change 9–11 cm with

Table 4

Changes in the four tidal constituents M2, S2, K1, O1, the MHW and the Maximum Range over a 15 day period with 2 m of Uniform SLR both assuming a fixed present day coastline (+2UF) and permitting the coastline to recede (+2UR). This subset of 40 of the 136 coastal cities with populations > 1 million is based on the locations with the 20 largest changes in MHW with a fixed coastline and with coastal recession (where MHW changes are top 20 for both coastal setups the next largest change is taken). Stars after the change value indicate a non-proportional response (outside +/−10%) with respect to the 0.5 m SLR change scaled according to the SLR.

COUNTRY, City/ Agglomeration	Present Day Exposure Ranking		M2 (cm)			S2 (cm)			K1 (cm)			O1 (cm)			MHW (cm)			Max Range (cm)		
	Population	Asset	Control	+2UF	+2UR	Control	+2UF	+2UR	Control	+2UF	+2UR	Control	+2UF	+2UR	Control	+2UF	+2UR	Control	+2UF	+2UR
ARGENTINA, Buenos Aires	64	52	78	-4	-51	68	-20	-47	13	-2	-3	22	0	-6	98	-15	-64	312	-46	-195
AUSTRALIA, Adelaide	123	103	54	-13	-31	73	13	38	23	-1	-1	21	0	-1	86	0	17	318	-4	11
BANGLADESH, Chittagong	39	72	153	16	-13	49	5	-6	20	0	-1	8	0	0	147	16	-13	433	43	-37
BANGLADESH, Dhaka	14	43	140	26	-1	41	9	0	20	0	0	8	0	0	134	25	-1	393	71	-1
BANGLADESH, Khulna	23	54	88	-4	19	34	-1	6	16	0	1	5	0	0	87	-4	19	266	-9	51
BRAZIL, Belém	72	79	251	28	-142	44	11	-23	9	1	-4	10	2	-4	233	28	-131	614	83	-340
BRAZIL, Porto Alegre	78	83	6	1	3	10	9	12	5	0	8	9	1	14	14	7	18	50	18	65
CAMEROON, Douala	110	128	65	-3	-15	33	-1	-8	9	0	0	2	0	0	70	-3	-16	204	-8	-46
CANADA, Montréal	84	55	109	23	154	160	-35	-92	24	0	-2	25	1	-2	182	-8	66	571	2	150
CHINA, Dalian	55	63	49	22	-1	15	4	-1	32	-2	-2	22	-1	-1	67	12	-3	197	47	-9
CHINA, Fuzhou Fujian	42	48	238	23	7	77	5	2	34	-1	-1	27	0	0	234	22	6	704	54	14
CHINA, Guangzhou Guangdong	2	11	116	-29	-29	60	-27	-13	48	-3	-4	38	-2	-3	121	-23	-19	480	-120	-94
CHINA, Shenzen	18	31	92	-17	-17	46	-18	-6	45	-2	-3	35	-1	-2	100	-11	-8	395	-74	-54
CHINA, Hangzhou	92	108	173	15	24	49	8	12	30	-1	1	24	-1	1	166	16	25	520	42	72
CHINA, Ningbo	34	40	64	35	21	19	10	6	26	1	2	20	0	1	68	28	20	232	88	60
CHINA, Shanghai	3	13	203	-22	-24	79	-5	-4	26	-1	-1	18	-2	-1	205	-21	-22	623	-59	-61
CHINA, Taipei	49	59	86	17	9	24	4	2	24	-1	-1	19	0	0	85	16	8	276	42	21
CHINA, Tianjin	12	25	59	25	8	14	5	2	29	1	1	23	0	2	67	12	1	225	60	24
CHINA, Xiamen	36	44	217	17	2	64	4	1	38	-2	-2	30	-1	-1	212	15	2	640	36	0
CHINA, Zhanjiang	40	45	101	-13	-10	54	-21	-4	47	-2	-2	37	0	-1	112	-12	-7	435	-69	-34
NORTH KOREA, Namp'o	87	121	171	18	-7	53	3	0	46	-3	-2	31	-1	0	167	12	-6	548	37	-18
DENMARK, Copenhagen	82	53	29	9	16	4	4	1	1	0	0	1	0	0	27	9	15	67	29	36
ECUADOR, Guayaquil	26	41	157	5	-75	49	7	-19	11	0	-2	3	0	-1	152	7	-71	428	23	-193
GERMANY, Hamburg	37	18	167	-2	-104	35	4	-18	4	0	-1	11	2	-2	156	-1	-96	425	7	-247
GUINEA, Conakry	70	113	159	-21	-15	54	-8	-5	8	0	0	4	0	0	156	-21	-15	435	-57	-41
INDIA, Calcutta	6	22	125	-12	-40	50	-4	-21	17	0	0	5	0	0	127	-12	-43	373	-31	-119
INDIA, Surat	24	46	200	11	39	123	4	-8	50	0	-1	35	0	-2	228	9	26	759	32	55
INDONESIA, Palembang	48	73	16	1	-10	5	2	-3	50	15	-3	43	7	-3	76	18	-10	192	43	-18
INDONESIA, Surabaya	68	88	190	-22	-46	78	-14	-28	45	1	6	36	1	4	194	-25	-50	651	-69	-136
IRELAND, Dublin	95	62	133	12	-24	36	5	-6	9	0	0	16	0	0	129	12	-22	363	34	-60
JAPAN, Hiroshima	44	24	163	-9	-50	79	-4	-32	29	0	1	22	0	2	175	-10	-58	539	-28	-146
MALAYSIA, Kuala Lumpur	35	33	128	4	-16	42	6	-3	30	0	-1	15	0	-1	127	6	-15	396	22	-42
MYANMAR,	22	60	162	32	-8	54	13	1	20	1	0	9	1	0	158	33	-6	471	92	-13

6

Table 4 (*continued*)

COUNTRY, City/ Agglomeration	Present Day Exposure Ranking		M2 (cm)			S2 (cm)			K1 (cm)			O1 (cm)			MHW (cm)			Max Range (cm)		
	Population	Asset	Control	+2UF	+2UR	Control	+2UF	+2UR	Control	+2UF	+2UR	Control	+2UF	+2UR	Control	+2UF	+2UR	Control	+2UF	+2UR
Rangoon																				
NETHERLANDS, Amsterdam	15	6	84	7 *	-38 *	18	5 *	-7 *	6	0 *	-1 *	16	2 *	-4 *	76	7 *	-33 *	228	24 *	-94 *
NETHERLANDS, Rotterdam	17	7	144	-9 *	-75 *	29	2 *	-14 *	7	0 *	-2 *	20	1 *	-5 *	131	-8 *	-69 *	376	-17 *	-185 *
SOUTH KOREA, Inchon	43	30	364	12 *	-13 *	109	8 *	3 *	42	-2 *	-1 *	31	-1 *	0 *	353	13 *	-10 *	1045	37 *	-22 *
UNITED KINGDOM, Glasgow	91	68	138	5 *	-30 *	37	3 *	-10 *	8	0 *	0 *	15	0 *	0 *	133	5 *	-29 *	376	17 *	-79 *
USA, Houston	67	36	66	-25 *	-33 *	16	13 *	-3 *	18	-2 *	-2 *	18	-1 *	-2 *	65	-15 *	-30 *	213	-31 *	-84 *
USA, New Orleans	10	3	1	6 *	3 *	0	2 *	1 *	11	7 *	12 *	12	10 *	8 *	16	14 *	16 *	46	41 *	42 *
VIETNAM, Ho Chi Minh City	5	27	111	-31 *	-40 *	56	-14 *	-31 *	67	-2 *	-15 *	54	-3 *	-10 *	128	-27 *	-46 *	480	-95 *	-171 *

a 1 m SLR if the change with 0.5 m SLR was 5 cm. Ratios > 1.1 (< 0.9) indicate that the response is above (below) proportional and a ratio < 0 indicates that the response has changed sign between the SLR scenarios and is also therefore non-proportional. All figures and tables referring to proportionality in this paper use this definition.

3. Results

For more detailed geographic descriptions of the results and additional figures please refer to Pickering (2014).

3.1. Effect of uniform SLR with a fixed coastline on the tides

This section presents results for the effect of uniform SLR on the tide assuming a fixed present day coastline (UF scenarios). The response of the four primary tidal constituents, M2, S2, K1 and O1, to a 2 m SLR is shown in Fig. 1a-d. The colour scales have limits scaled in proportion to the constituents' equilibrium tidal amplitudes in order to show more clearly the changes in the smaller amplitude constituents. Fig. 1a shows the M2 response to be widespread globally with spatially coherent non-uniform amplitude changes of both signs in many shelf seas. Response in the open ocean, where the relative depth change with SLR is small, is generally of a much smaller magnitude but with a much greater horizontal length scale. Significant but localised changes at the coast may occur but these are not always easily identifiable in the global plots. Changes at large coastal city locations can be seen in the M2+2UF column of Table 4 (full table in SM). At 14 locations amplitude changes of ≥20 cm or ≤−20 cm (≥10% of the SLR imposed) occur, with the largest increase (35 cm) at Ningbo and the largest decrease (−31 cm) at Ho Chi Minh City.

The S2 constituent (Fig. 1b) also shows a global response of non-uniform coherent changes of both signs in many shelf seas with a slightly reduced overall magnitude compared with M2. Comparison of the M2 and S2 constituent responses show some areas to have greater and lesser responses. Furthermore in some locations M2 and S2 changes are of the same sign, whereas in others the changes are of opposing sign. Changes at large coastal city locations can be seen in the S2+2UF column of Table 4. At 12 locations amplitude changes of ≥10 cm or ≤−10 cm (≥5% of the SLR imposed) occur, with the largest increase (13 cm) at Adelaide and the largest decrease (−35 cm) at Montreal.

The K1 response to SLR (Fig. 1c) also shows non-uniform spatially coherent changes of both signs but with a more limited geographic spread mostly confined to Asia where the present day K1 amplitudes are at their largest. Few coastal cities show significant (≥5 cm or ≤−5 cm) change in K1 amplitude, except Palembang and New Orleans with changes of 15 cm and 7 cm respectively.

The effect of SLR on the O1 constituent (Fig. 1d) shows similar spatial characteristics to that of K1, but with a reduced response in the Persian Gulf and the Timor Sea and a change in the sign of the response in the Java Sea. Again, the only coastal cities experiencing a significant response are Palembang and New Orleans (7 cm and 10 cm respectively).

The mean high water (MHW) change shows the combined effect of the changes to the tidal constituents averaged over a 15 day period. Fig. 2a shows the MHW change to behave in a spatially similar way to changes in the tidal constituents, with areas of both increase and decrease, largely in the shelf seas. The horizontal length scale of the change is again much larger in the open ocean than on the shelf. Comparison of the MHW change plots for 0.5 m and 1 m (not shown) and the 2 m SLR maximum range change plot with 2 m SLR (Fig. SM10) showed almost identical spatial characteristics to Fig. 2a. The 2 m SLR MHW changes can therefore also be used as an indication of the nature of the MHW change with 0.5 m and 1 m SLR, although the magnitude of the change will be smaller and may not fit our fairly rigorous definition of proportionality (see Section 3.3). The same goes

Table 5

Changes in MHW and Maximum Range over a 15 day period with 0.5, 1 and 2 m of Uniform SLR assuming a fixed present day coastline (UF). This subset of 40 of the 136 coastal cities with populations > 1 million is based on the locations with the 40 largest changes in MHW with 2 m SLR. Stars after the change value indicate a non-proportional response (outside +/- 10%) with respect to the 0.5 m SLR change scaled according to the SLR.

COUNTRY, City/Agglomeration	Present Day Exposure Ranking		MHW (cm)						Max Range (cm)					
	Population	Asset	Control	+0.5UF	+1UF		+2UF		Control	+0.5UF	+1UF		+2UF	
ARGENTINA, Buenos Aires	64	52	98	−7	−12	*	−15	*	312	−20	−35	*	−46	*
AUSTRALIA, Melbourne	100	74	74	2	4		7		269	4	8		17	
BANGLADESH, Chittagong	39	72	147	3	7	*	16	*	433	8	19	*	43	*
BANGLADESH, Dhaka	14	43	134	6	13		25		393	18	35		71	
BRAZIL, Belém	72	79	233	9	16	*	28	*	614	26	48		83	*
CANADA, Montréal	84	55	182	0	1	*	−8	*	571	12	23		2	*
CHINA, Dalian	55	63	67	3	6		12		197	10	21		47	*
CHINA, Fuzhou Fujian	42	48	234	5	10		22		704	12	26		54	
CHINA, Guangzhou Guangdong	2	11	121	−7	−12	*	−23	*	480	−30	−62		−120	
CHINA, Shenzen	18	31	100	−2	−4	*	−11	*	395	−15	−35	*	−74	*
CHINA, Hangzhou	92	108	166	4	8		16		520	11	21		42	
CHINA, Ningbo	34	40	68	8	15		28		232	24	46		88	
CHINA, Qingdao	57	65	93	2	5		9		301	5	9		19	
CHINA, Shanghai	3	13	205	−6	−11		−21	*	623	−15	−31		−59	
CHINA, Taipei	49	59	85	4	8		16		276	10	20		42	
CHINA, Tianjin	12	25	67	4	7		12	*	225	18	33		60	*
CHINA, Xiamen	36	44	212	4	7		15		640	8	17		36	
CHINA, Yantai	115	119	33	0	1	*	7	*	118	5	11	*	28	*
CHINA, Zhanjiang	40	45	112	−4	−7	*	−12	*	435	−20	−39		−69	*
NORTH KOREA, Namp'o	87	121	167	3	5		12	*	548	9	18		37	
DENMARK, Copenhagen	82	53	27	8	15		9	*	67	21	36	*	29	*
ECUADOR, Guayaquil	26	41	152	3	5	*	7	*	428	10	17	*	23	*
GUINEA, Conakry	70	113	156	−7	−13	*	−21	*	435	−20	−35	*	−57	*
INDIA, Calcutta	6	22	127	−3	−6		−12	*	373	−9	−17		−31	*
INDIA, Bombay	1	17	148	−2	−5		−8	*	489	−5	−10		−16	*
INDIA, Surat	24	46	228	2	4		9	*	759	7	15		32	
INDONESIA, Palembang	48	73	76	6	10	*	18	*	192	13	24		43	*
INDONESIA, Surabaya	68	88	194	−7	−13		−25		651	−17	−33		−69	
IRELAND, Dublin	95	62	129	3	6		12		363	8	17		34	
JAPAN, Hiroshima	44	24	175	−3	−5		−10	*	539	−8	−15		−28	*
KUWAIT, Kuwait City	101	84	99	2	5	*	9	*	384	10	22		36	*
MYANMAR, Rangoon	22	60	158	8	16		33		471	23	46		92	
NETHERLANDS, Rotterdam	17	7	131	0	−3	*	−8	*	376	0	−7	*	−17	*
PANAMA, Panama City	99	109	237	−2	−4		−7		662	−4	−10		−19	
SOUTH KOREA, Inchon	43	30	353	4	7		13		1045	11	21		37	*
SINGAPORE, Singapore	96	75	31	2	4		8	*	105	5	10		20	
USA, Houston	67	36	65	1	−3	*	−15	*	213	6	−9	*	−31	*
USA, New Orleans	10	3	16	3	7	*	14	*	46	8	21	*	41	*
URUGUAY, Montevideo	94	96	20	3	6	*	11	*	58	12	25		48	
VIETNAM, Ho Chi Minh City	5	27	128	−9	−15	*	−27	*	480	−26	−48		−95	*

for the maximum range changes with 2 m SLR although the magnitudes will be larger. Regional enlargements of Fig. 2a (and Fig. 2b) for Europe, Africa, Australia, North and South America can be found in Figs. SM4-9. An example showing the substantial MHW response in Asia is given in Fig. 3.

Table 5 shows the 40 largest MHW changes at coastal cities for the +2UF scenario. At 10 cities MHW changes of ≥20 cm or ≤−20 cm occur, with the largest increase (33 cm) at Rangoon and the largest decrease (−27 cm) at Ho Chi Minh City. The largest increase and decrease at locations with top 20 population exposure (Nicholls et al., 2008) are 25 cm at Dhaka and −27 cm at Ho Chi Minh City. The largest increase and decrease at locations with top 20 asset exposure are 14 cm at New Orleans and −23 cm at Guangzhou Guangdong. Another way of considering amplitude changes is as a percentage of their control amplitude; the change at Ningbo of 28 cm, for example, is 41% of the Control MHW. Table 5 also shows the MHW change at these cities with 0.5 m and 1 m SLR. At all the cities shown except Montreal, Copenhagen and Houston the MHW changes are of the same sign and increase incrementally from 0.5 to 1 m and from 1 m to 2 m SLR. With 1 m SLR there are 13 cities with MHW changes of ≥10 cm or ≤−10 cm, with the largest increase (16 cm) again at Rangoon and the largest decrease (−15 cm) again at Ho Chi Minh City. With 0.5 m SLR there are 13 cities with MHW changes of ≥5 cm or ≤−5 cm, with the

largest increase (9 cm) at Belem and the largest decrease (−9 cm) again at Ho Chi Minh City.

Table 5 also shows that the maximum range changes with 2 m SLR. These are > 40 cm or < −40 cm at 21 cities. Large increases are found at Rangoon (92 cm), Ningbo (88 cm) and Belem (83 cm) whereas large decreases are seen at Guangzhou Guangdong (−120 cm), Ho Chi Minh City (−95 cm) and Shenzen (−74 cm). As with MHW changes, at all locations except Montreal, Copenhagen and Houston the maximum range changes are of the same sign and increase incrementally from 0.5 to 1 m and from 1 m to 2 m SLR. With only 0.5 m SLR maximum range changes are still substantial, with changes of ≥25 cm or ≤−25 cm (50% of the SLR imposed) occurring at 3 cities.

3.2. Effect on tides of including coastal recession with uniform SLR

The MHW changes presented in Section 3.1 for +2UF (Fig. 2a) can be compared to those obtained with the same SLR but allowing recession of the coastline in areas of low lying land (Fig. 2b). Large scale differences in the tidal response can be seen between the two coastline assumptions, with many MHW changes swapping sign when coastal recession is permitted. A few areas maintain changes of the same sign and a similar magnitude in both coastal conditions and in some regions the sign of the MHW change remains the same but the

magnitude is amplified. It is important to note that in the coastal recession SLR cases there are areas inland of the original coastline that now experience tides for the first time. These grid cells have their (now calculable) MHW value plotted on the positive part of the Fig. 2b differences colour scale. Only the largest recession areas are visible (e.g. Amazon region and southern Papua) however regional enlargements of Fig. 2b can be found in the SM.

The changes in the four tidal constituents, MHW and maximum range at 40 coastal cities for the +2UR scenario are given in Table 4. The changes with 2 m SLR and a fixed coastline (+2UF) were presented in Section 3.1 so the focus here will be where changes are substantially different in the coastal recession scenario (+2UR). With recession there are now 20 cities where M2 amplitude changes of ≥20 cm or ≤−20 cm occur, 12 of which are at new locations compared to the fixed coastline case. Of these 20 substantial changes, 16 are decreases in the recession scenario (compared with 6 from 14 in the fixed coastline scenario). The largest M2 increase and decrease with recession is now 154 cm at Montreal and −142 cm at Belem. Changes to the amplitude of the S2 constituent of ≥10 cm or ≤−10 cm occur at 15 locations, 8 of which are at new locations compared to the fixed coastline case. Of these 15 substantial changes, 12 are decreases in the recession scenario (compared with only 7 from 12 in the fixed coastline scenario). The largest S2 increase and decrease with recession is now 38 cm at Adelaide and −92 cm at Montreal. With recession, significant (≥5 cm or ≤−5 cm) change in K1 amplitude occurs at 3 locations where with a fixed coastline the change was insignificant and one where it was significant. The SLR induced change in the O1 constituent with coastal recession is significant (≥5 cm or ≤−5 cm) at 4 locations where with a fixed coastline the change was insignificant and one where it was significant.

With coastal recession, MHW change of ≥20 cm or ≤−20 cm now occurs at 18 cities, 13 of which are at new locations compared to the fixed coastline (Table 4). Of these 18 substantial changes, 14 are decreases in the recession scenario (compared with 5 from 10 in +2UF). The largest MHW increase and decrease with recession is now 66 cm at Montreal and −131 cm at Belem. With coastal recession the largest MHW increase and decrease at locations with top 20 population exposure are respectively 16 cm at New Orleans and −43 cm at Calcutta. The largest MHW increase and decrease at locations with top 20 asset exposure are 16 cm at New Orleans and −96 cm at Hamburg. Maximum range changes are > 40 cm or < −40 cm at 26 cities: large maximum range increases are seen at Montreal (150 cm), Hangzhou (72 cm) and Porto Alegre (65 cm), whilst large maximum range decreases are predicted at Belem (−340 cm), Hamburg (−247 cm) and Buenos Aires (−195 cm).

Comparisons at cities of MHW changes at higher SLR scenarios of 5 m and 10 m with fixed coastlines and with coastal recession are given in Table SM2.

3.3. Proportionality of the tidal response

Using the definition of proportional tidal change (see Section 2.3) Table 6 provides a global overview of the proportionality of change at points with significant (> 5 cm or < −5 cm) MHW change for +1UF, +2UF, +5UF and +10UF. Table 6 shows that the portion of cells displaying a proportional change decreases with SLR. The portion of cells classified as strongly non-proportional (ratios of < 0, 0−0.5 and 1.5+) however, increases with SLR. The largest category of model cells is proportional for both 1 m and 2 m SLR, and that mode moves towards higher proportionality ratios with further SLR. In other words changes are more proportional at lower SLR scenarios and become increasingly above proportional at higher SLR scenarios.

The spatial distributions of the significant MHW change points (analysed in Table 6) for +1UF and +5UF in Europe are shown in Fig. 4a and b (plots for the other regions globally can be found in Figs. SM11-15). +5UF is presented, rather than +10UF, as it is considered more plausible in the context of long timescale SLR (Church et al., 2014). Not surprisingly there are larger areas where the MHW changes exceed ± 5 cm in the 5 m SLR plot than in the corresponding plot for only 1 m of SLR. This is supported by the total numbers of significant cells globally in Table 6 (~13,000 with 1 m SLR compared with ~104,000 with 5 m SLR). Changes that are proportional (green) with 1 m SLR in the Celtic Sea and western English Channel become slightly below and above proportional respectively with 5 m SLR. In the southern North Sea, the near proportional and proportional changes with 1 m SLR become below proportional with 5 m SLR. In the Baltic Sea regions of proportional and near proportional change with 1 m SLR become areas of sign change of the MHW response with 5 m SLR. The other regions globally generally show proportional cells transitioning to non-proportional from +1UF to +5UF.

In Tables 4, 5, non-proportionality of the changes in the tidal properties presented for individual port cities is indicated by the stars after the change value. Using the full versions of these tables with all 136 coastal city results (see SM) the percentage of cities with non-proportional change for each tidal property and SLR scenario is given in Table 7. Similarly to the MHW results in Table 6 all properties have a tendency towards non-proportionality with increasing SLR. This is summarised in the increasing mean values as SLR increases. The low K1 constituent mean across the SLR scenarios shows it to be the most proportional property; conversely the high S2 mean shows it to be the least proportional property. In Table 5 this trend towards more non-proportional changes (stars) at the higher SLR is also shown.

Related to the question of tidal response proportionality is that of tidal change symmetry about the present day sea-level. This was tested by comparing the 2 m sea-level fall (SLF) and 2 m SLR changes. In the −2UA case the coastline is allowed to advance so it might be expected
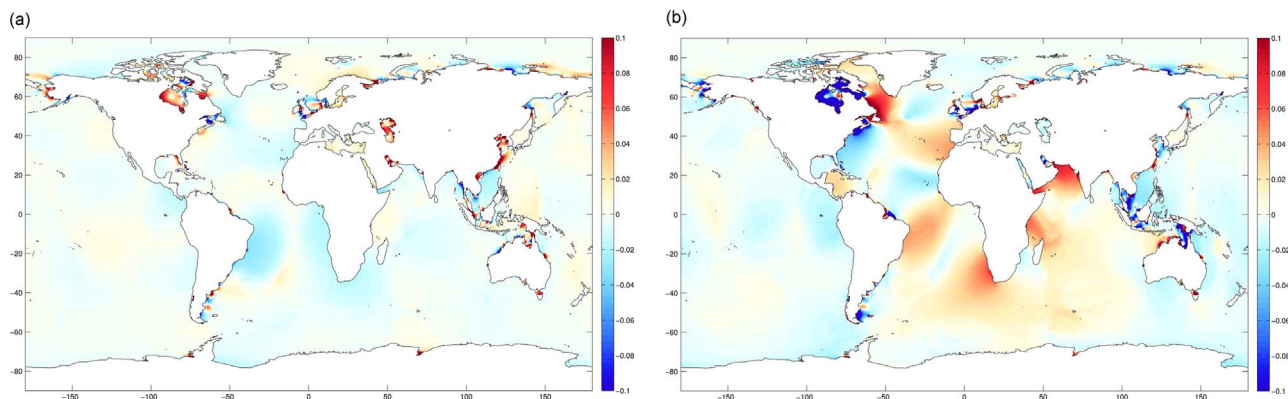

Fig. 2. (a) Change in MHW (m) with 2 m of uniform SLR assuming a fixed present day coastline (+2UF) (increases- red, decreases- blue). For coastal city changes see Tables 4, 5. (b) Change in MHW (m) with 2 m of uniform SLR permitting coastal recession (+2UR), except around Antarctica (increases- red, decreases- blue). For coastal city changes see Table 4. For newly wet areas in the SLR scenario the now calculable MHW values are plotted on the positive part of the colour scale.
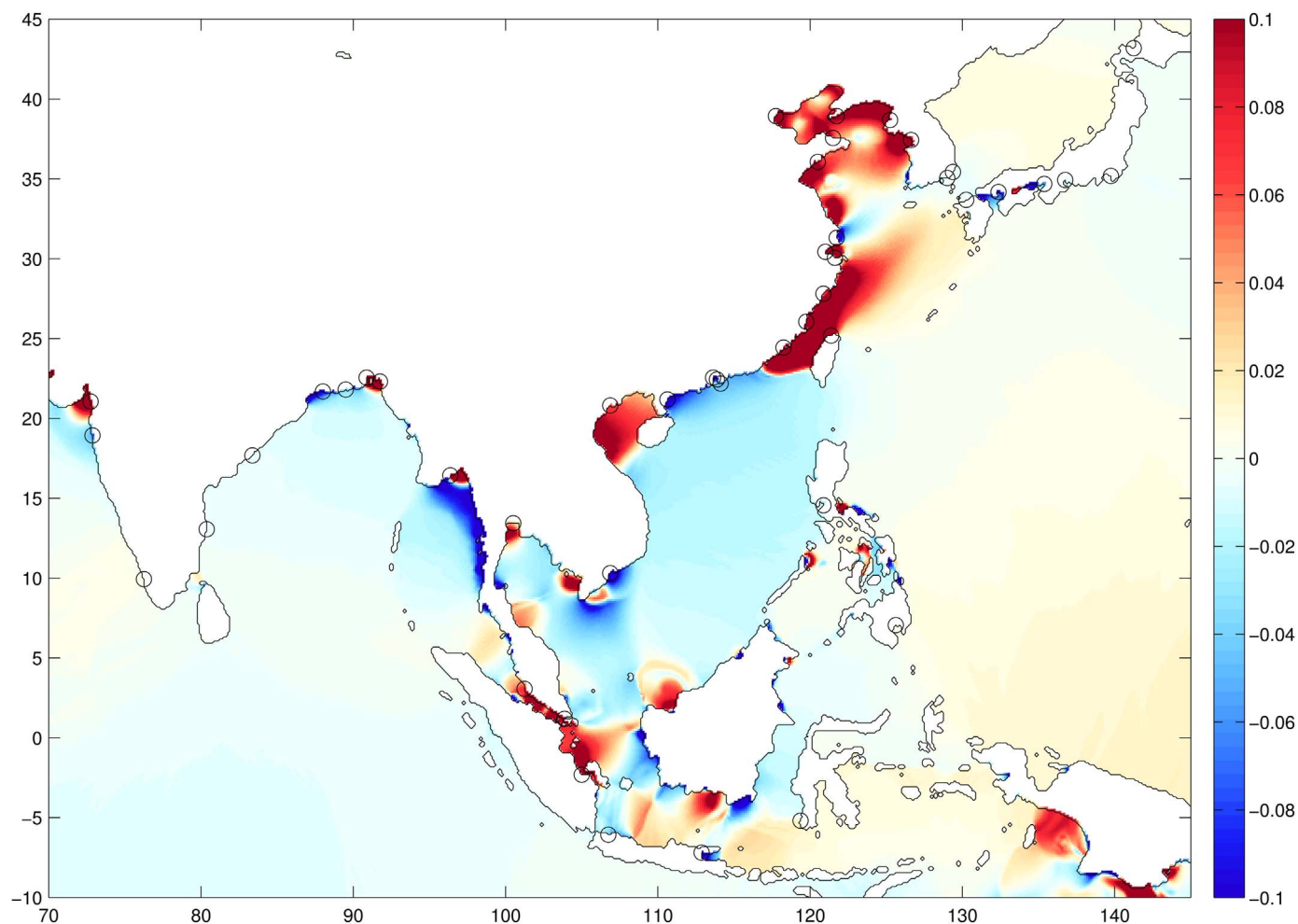
Fig. 3. Asian change in MHW (m) with 2 m of uniform SLR assuming a fixed present day coastline (+2UF) (increases- red, decreases- blue). For coastal city changes, marked by the black circles, see Tables 4, 5. (Regional zoom of Fig. 2a).

Table 6
Percentage of total significant (> +/ < - 5 cm) MHW change cells in each proportionality category for various uniform SLR scenarios with a fixed coastline assumption (UF) (geographic distribution of points given in Fig. 4, SM11-15). The proportionality ratio for each cell is given by the ratio of the MHW change for the SLR scenario to the 0.5 m SLR MHW change which is then normalised for each SLR scenario so that proportional change is given by a ratio of 1 (+/- 0.1). Ratio values < 0.9 (> 1.1) or < 0 show a below (above) proportional change or sign change of the MHW response in the SLR scenario.

Norm. Proportionality Ratio	Percentage of Sig. MHW Response Cells in each Proportionality Category (%)			
	+1UF	+2UF	+5UF	+10UF
< 0 (Sign Change)	1	4	9	19
0–0.5	1	3	6	6
0.5–0.9	24	27	19	18
0.9–1.1 (Proportional)	61	34	19	11
1.1–1.5	9	19	25	10
1.5+	4	12	21	37
Total Sig. Cells (> +/ < - 5 cm)	12871	32166	104106	278050

to be to some extent symmetrical with the +2UR case. The MHW change with −2UA is shown in Fig. SM16. In most areas the −2UA scenario has spatial patterns and magnitudes of change that are similar but of opposing sign to the +2UF results. There are some limited areas where the symmetry is better with the +2UR MHW change. Table SM3 gives MHW change at cities with −2UA as well as the two coastal conditions with 2 m SLR for comparison. At 37 of the 40 locations a

change of the opposing sign to the −2UA change can be found in one of the two 2 m SLR coastal setups, suggesting approximately symmetric tidal change. The −2UA change is more symmetrical with the +2UF scenario at 26 locations and with +2UR case at the other 14.

3.4. Effect on MHW of non-uniform SLR due to initial elastic response

This section describes the tidal response to non-uniform perturbations of the SLR resulting from IER. Three scenarios are chosen, all of which imply a 2 m global mean sea level rise. The three scenarios have distinct spatial fingerprints based on ice sheet melt contributions that are (1) 100% from Greenland (Fig. SM17), (2) 100% from Western Antarctic (Fig. SM18) and (3) 50% from Greenland and 50% from Western Antarctica (Fig. 5). The first two figures are included in SM as they were published in Mitrovica et al. (2001) whereas Fig. 5 is a new combination of the fingerprints. The scenarios with 2 m of SLR from Greenland or Western Antarctica both have above (below) average values of SLR in the far (near) field of the ice mass loss and even SLFs in very close proximity to the mass loss. When these fingerprints are combined with 1 m SLR from each ice sheet the above average SLR radiates from equatorial regions with below average SLR at both of the poles.

The effect on the MHW of these IER SLR perturbations is initially assessed with a fixed present day coastline but allowing coastal advancement (drying where sea level falls). The MHW changes with 2 m SLR from Greenland or Antarctica represent the limits of the scenarios explored so we present these rather than the combined SLR fingerprint as its MHW response is some combination of the two. In the
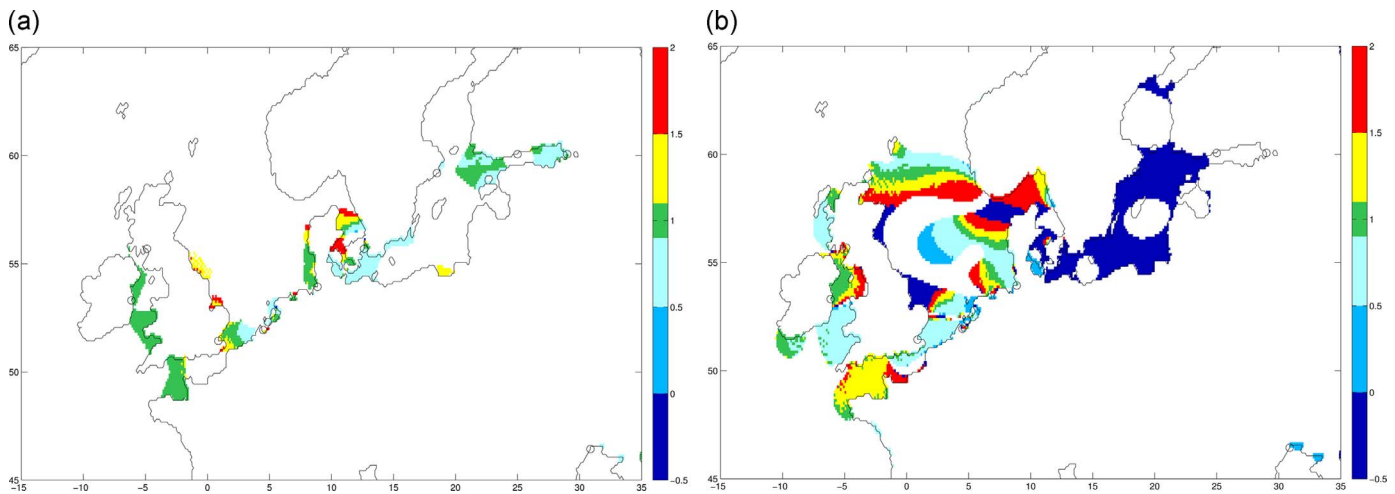
(a)

(b)

Fig. 4. a. European normalised proportionality ratio of the significant MHW change with (a) 1 m uniform SLR (+1UF) and (b) 5 m uniform SLR (+5UF) to the MHW change with 0.5 m uniform SLR (+0.5UF) assuming a fixed coastline. Proportional change is given by a ratio of 1 (+/- 0.1). Ratio values < 0.9 (> 1.1) or < 0 show a below (above) proportional change or sign change of the MHW response in the SLR scenario. Insignificant MHW Changes (< +/ > - 5 cm) are masked out. Black circles mark coastal cities.

Table 7
Percentages of all the 136 coastal cities analysed where the change in tidal constituent, MHW or maximum range is defined as non-proportional (> +/ < - 10%) with respect to the scaled 0.5 m SLR change. Mean values for constituents, MHW and maximum range as well as for each uniform fixed coastline (UF) SLR scenarios are given.

Property	Percentage of 136 Coastal Cities with Non-Proportional Change (%)				
	+1UF	+2UF	+5UF	+10UF	Mean
M2	56	79	89	93	79
S2	71	85	93	93	85
K1	43	72	88	93	74
O1	63	82	90	90	81
MHW	57	79	94	93	81
Max Range	51	74	89	93	77
Mean	57	79	90	93	

Greenland melt case (+2NUGF) the MHW response (Fig. 6a) differs from the uniform SLR response (Fig. 2a) particularly in the near field with a change in sign of the response in the Hudson Bay and Northwest Passages and a diminished response on the European Shelf and along the north coast of Russia. The MHW change in the Western Antarctic melt case (+2NUWAF) (Fig. 6b) is for the most part almost identical to the uniform SLR response (Fig. 2a) except for in the near field with a substantial reduction in the intensity of the response on the Patagonian Shelf. The MHW change in the IER scenario with melt from both ice sheets (+2NUBF) is given in Fig. SM19a. In all three IER SLR scenarios the MHW change within 30 degrees of the equator is largely consistent. This means regions such as Asia experience substantial changes to tidal characteristics, regardless of the IER scenario, whereas the effect of SLR on tides in higher latitude areas is more IER scenario dependent.

The MHW change values with non-uniform SLR at large coastal cities are presented in Table 8. A table showing the local SLR imposed at each city is given in Table SM1 In many locations the difference between the MHW responses in the IER scenarios is only of the order a few centimetres but they do show the expected increase (decrease) in MHW response when localised SLR is above (below) the 2 m average. Some higher latitude cities such as Montreal and those on the European Shelf show more marked differences. At all 22 Asian cities the uniform SLR MHW changes either remain the same or are intensified in all three IER scenarios. Higher than global mean SLR in the non-uniform SLR scenarios in addition to augmented tidal changes could pose substantially increased flood risk: for example, a uniform SLR of 200 cm and MHW increase of 28 cm at Ningbo becomes a SLR of 233 cm and MHW increase of 32 cm in the

Greenland melt scenario.

To assess the tidal response associated with non-uniform SLR and also permitting coastal recession, a 2 m average SLR scenario with 1 m of melt from each of the ice sheets allowing coastal recession with SLR (as well as drying where SLFs) was tested. The MHW change under this +2NUBR scenario is included in Fig. SM19b and can be compared with the +2UR scenario (Fig. 2b). Table 8 also shows the differences between the +2UR and the +2NUBR scenarios. With a fixed coastline the difference between the uniform SLR and IER Both scenarios is ≥5 cm at only 3 of 40 cities whereas allowing coastal recession the difference is ≥5 cm at 16 of 40 cities. This shows the coastal condition to be as important in the IER scenario as it was for Uniform SLR. In the +2NUBF scenario there are 10 substantial (≥20 cm or ≤−20 cm) changes (5 of which are decreases), whereas in the +2NUBR scenario, 18 are substantial (16 being decreases). These +2NUBF and +2NUBR scenarios show there to be a larger number of substantial changes (with a greater portion of them being decreases) when coastal recession is included - the same pattern identified in the uniform 2 m SLR scenarios (Section 3.2).

3.5. Implications for marine renewable energy

The criteria for a presently viable location for tidal energy extraction given in Section 2.3 were used to create a mask that was then applied to the maximum range change results with +2UF. The European plot in Fig. 7 indicates that under this SLR scenario there are large decreases in available future energy in the Gulf of St. Malo (France), Bristol Channel (England), west coast of Scotland and east coast of England; increases are suggested in the eastern English Channel, eastern Irish Sea and north coast of East Anglia. For other tidal renewable changes globally see Pickering (2014). It should be noted that the trends in the maximum tidal range still vary with differing SLR scenarios and coastline assumptions (e.g. the tidal response in the Hudson Strait).

4. Discussion

4.1. Discussion of tidal changes

Our results show that future sea level rise (SLR) will significantly affect global tides. The different SLR scenarios allow us to rank the factors that influence tidal change. The most important factor is the amount of SLR imposed. Following that is the inclusion (or not) of moving coastlines (as a proxy for actual coastal recession with SLR), and
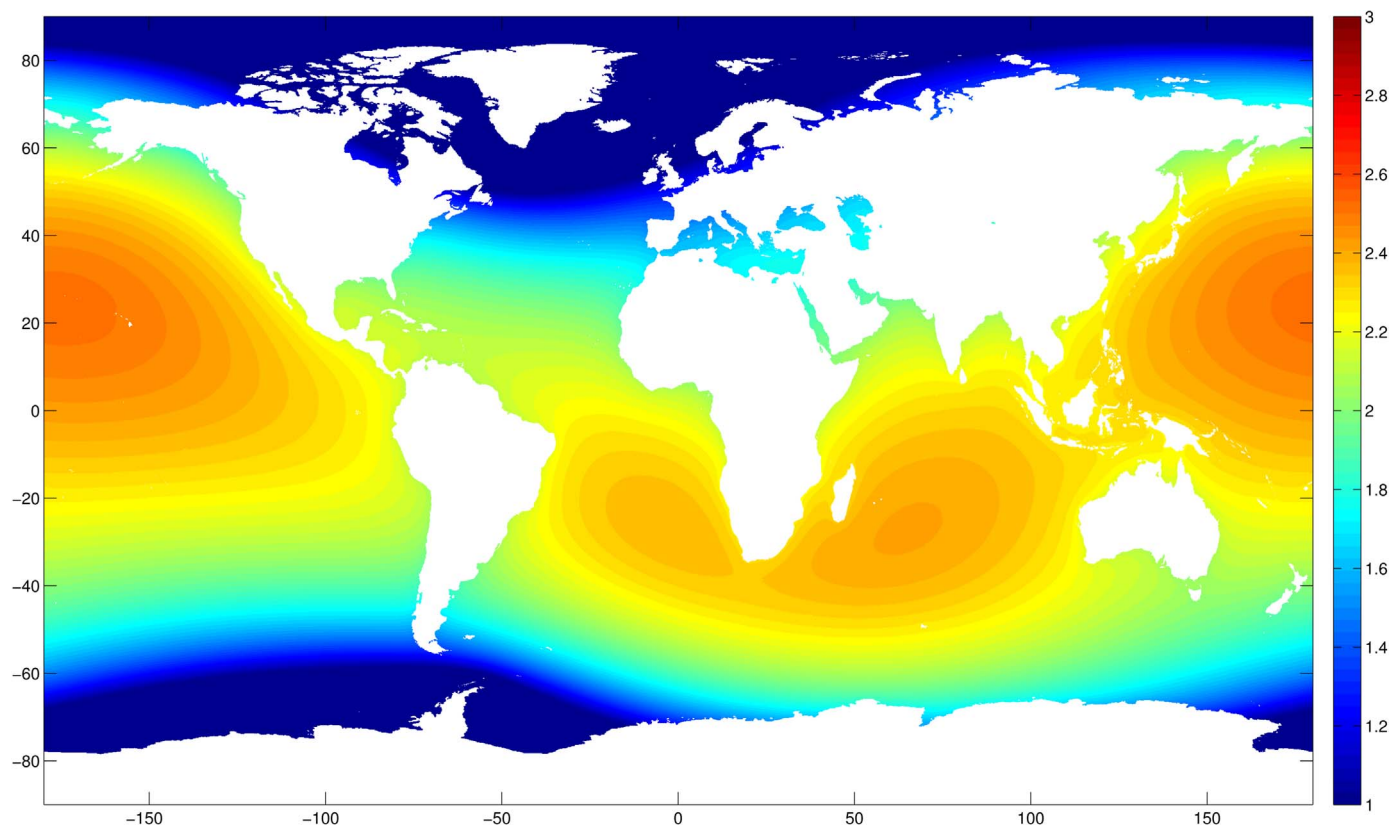
Fig. 5. The SLR perturbation (m) applied to the model for the 2 m average SLR non-uniform initial elastic response scenario with uniform ice sheet melt in both Greenland (1 m) and Western Antarctica (1 m) (+2NUB). In the near field of the areas of the mass loss sea-level change can be negative. For coastal city SLR values see Table SM1. Data courtesy of Mitrovica et al. (2001).

the least influential factor is the global pattern of non-uniform SLR.

The changes in tidal constituents (Section 3.1) showed the two main semidiurnal constituents in some areas to exhibit changes of opposing signs, whilst in other places changes were of the same sign. When considering the phasing of these constituents the consequence of the opposing (same) signs of change is a reduced (increased) effect on the spring tidal amplitude and increased (reduced) effect on the neap tidal amplitudes. Both changes have implications for flood risk. Positive, same sign changes would cause an increase in the spring tide HWs thus increasing the height of extreme water levels. Opposing sign changes can potentially increase the neap tide range, thus raising the average tidal range which could have consequences when combined with other flood drivers (e.g. storm surge or river discharge). Changes in spring and neap HWs will often be larger than the mean high water (MHW) changes presented.

The reason why the M2 and S2 constituents respond with opposite signs in the same SLR scenario for certain regions may be due to an alteration in the natural period of oscillation. For example, in the English Channel for the +2UF scenario the M2 constituent amplitude decreases whereas the S2 amplitude increases, suggesting the natural period of oscillation is moving away from the M2 period and towards the S2 period. The English Channel resonance is described by a half-wave oscillator through Merian's formula ($T = 2\,L/\sqrt{gH}$) (Merian, 1828). Based on the model topography we calculate a channel length (L) of 476.6 km and an average depth (H) of 47.4 m. A 2 m SLR would change T for this channel from 12.28 h to 12.03 h; closer to that of S2 (12 h) and further from M2 (12.42 h). It is interesting to note that the changes to the diurnal K1 (23.94 h) and O1 (25.82 h) constituents (Table 4 +2UF) are of the same sign at 39 of 40 cities. The diurnal constituent changes having a greater tendency to be of the same sign will increase HW changes during tropic tides when diurnal tides are at their maximum.

In this paper we have focused largely on the 2 m SLR scenario because (1) it represents a plausible high-end scenario for SLR (e.g. Jevrejeva et al., 2014), (2) the characteristics of the changes are largely representative of those for 0.5 m and 1 m SLR, and (3) the SLR is large enough to test domain changes with a moving coastline to represent coastal recession.

The majority of the large MHW responses to SLR are in shelf seas, with the sign of change varying spatially on shelves with multiple amphidromes. In contrast to this are the smaller magnitude but far greater horizontal length scale MHW decreases which extend across the Atlantic (Fig. 2a). As the relative depth change in these open ocean areas is small the changes are more likely to result from a change in the interaction between the shelf and ocean tide. Arbic et al. (2009) show that resonant ocean tides are strongly affected by resonant shelves, generally causing reductions to the tide, with a greater back effect for a weakly damped shelf. Reductions in the energy dissipation at the bed (and hence damping) are found on various shelf seas adjacent to these widespread areas of decrease (Fig. SM20a) adhering to the theory of Arbic et al. (2009). The ocean tidal response to many of the SLR scenarios is particularly marked in the Atlantic and western Indian Oceans with less of a response in the other oceans. This is potentially a result of the adjustment of the deep ocean tide, caused by the aforementioned altered shelf tide back effect, moving it closer to the natural modes of oscillation of these oceans (see Platzman et al., 1981).

Although our simulation of coastal recession affects the tidal change estimates substantially, the two coastline setups (fixed and recession) represent the limits of the problem. Whether the coastline is permitted to recede globally in 100 to 200 years depends on complex regional future socio-economics and coastal management practices that cannot be predicted. Coastal recession will have considerable flood impacts for coastal communities even though the substantial tidal changes in wet areas in both the present day and recession SLR scenarios were found

to be predominately decreases. The larger number of cities with significant MHW decreases in the +2UR case is clear from the cumulative frequency distributions (CFDs) presented in SM. The results also showed there to be tendency for the MHW changes to swap sign between the two coastline scenarios: this is particularly important for flood risk. In the areas where MHW change switches from an increase to a decrease (when coastal recession is permitted) there is a strong argument to give preference to managed retreat because by choosing to engineer large scale sea walls (fixed coastline) the tidal amplitude is increased. Furthermore, by engineering sea walls in these regions to protect against the SLR (and consequently amplified tide) the residual risk in the event of a failure of the defences is also increased (e.g. Hanson et al., 2011).

Coastal recession, represented here by domain change, not surprisingly has a substantial effect on the natural period (T) of oscillation of a channel. Using the English Channel half wavelength resonance example given earlier, a hypothetical increase in the channel length of just two grid cells (~28 km) with 2 m SLR causes an increase in period approximately twice as large as the decrease caused by 2 m SLR alone. The tendency for the tidal changes to swap sign between the +2UF and +2UR scenarios is likely due to the fact that SLR alone decreases T whereas SLR plus recession increases it. Furthermore the effect of recession on T will be further amplified for areas governed by quarter wavelength resonances (T=4 L/√gH) such as the Bay of Fundy and the Bristol Channel where one finds the world's largest tides. The tidal changes swapping sign between the +2UF and +2UR scenarios in deep water regions such as the Atlantic is explicable through similar reasoning. A simple scaling argument shows the effect of domain change with coastal recession on T in the ocean is at least as important as that of SLR. For example in 2000 m deep water the dynamic effect of 2 m SLR is to increase C=√gH by 0.07 m/s, tidal forcing periods are fixed, so the M2 constituent wavelength must also increase by approximately 3.1 km. This is less than a quarter the length of a grid cell (~14 km)- the minimum increment by which basin geometry increases with coastal recession. Another clear example of change in the sign of the ocean tide response can be seen in the northern Arabian Sea, where the adjacent and opposing large Persian Gulf tidal response also changes sign between the two coastline setups.

Changes in all tidal properties are shown to be increasingly non-proportional with increasing SLR, with a tendency towards an above proportional MHW response with higher SLR. These results emphasise that interpolation or extrapolation of the tidal changes from one SLR scenario to another will often be a poor assumption for planning purposes. There are a number of reasons why tidal changes are not expected to be proportional (i.e. scalable with SLR): (1) as the tidal wave speed increases with SLR, and the amphidromic points are shifted, the response at the coast is not a simple function of SLR; (2) the movement of the amphidrome is two dimensional and the

curvature of corange lines leads to a complex response; (3) as an amphidrome moves past a fixed coastal point with SLR the amplitude will first decrease (as it gets closer) then increase (as it moves away); (4) bathymetric and topographic slopes are not constant (as shown by non-proportional land areas newly wetted areas in UR scenarios Table 3).

The spatially non-uniform SLR from initial elastic response (IER) shows particular influence on the tidal response. IER SLR peaks in the mid ocean have a negligible effect. Where all three IER scenarios result in above average SLR in coastal regions (e.g. Asia) then the tidal response is substantial regardless of the scenario. Where tidal response is an increase, IER compounds the effect with both a larger tidal amplitude increase and an above average SLR. This compounding effect occurs at many Asian cities with the MHW increase being augmented by a few centimetres and the SLR increasing above the average (of the order) 20 cm (the primary effect). From the differences between the MHW changes in the IER scenarios we can also see that it is regionally imposed SLR not the global mean that drives the resulting tidal changes. This relatively localised effect of SLR on the tide means that spatially variable SLR caused by other processes, the projections of which are uncertain (Slangen et al., 2014), are also likely to influence the extent of regional tidal changes.

Comparison of the European OTISmpi M2 tidal changes with 2 m SLR (Fig. SM22a) to those of the regional modelling study by Pickering et al. (2012) shows good agreement. Furthermore, this global study shows that changes in the global model on the shelf edge (in the vicinity of the regional model's open boundary) are negligible. This supports the assumption (made in previous regional modelling studies) of maintaining constant tidal forcing at the open boundary with SLR. The weaker agreement between the two models with 10 m SLR (see Fig. SM22b) suggests that this assumption will break down at very high SLR scenarios. Improved grid resolution will always improve tidal results and the availability of well-resolved global models will eventually eliminate the need for regional models.

Globally the results of our model (Fig. SM21) are generally comparable with those of other studies (e.g. Green, 2010). Other regional comparisons for the European Shelf (see Figs. SM23 & 24) show somewhat similar patterns of M2 amplitude change to Ward et al. (2012) for +2UR and +5UR cases, and to Pelling et al. (2013a) for +2UR and +2UF cases. Comparisons of M2 amplitude change with Pelling et al. (2013b) for the Bohai Sea shows a similar response for the +2UR case but poorer agreement for the +2UF case where change outside the regional model's domain appear to influence the OTISmpi Bohai Sea response (Fig. SM26). The response of the astronomic tidal range in the Gulf of Maine (Fig. SM27) is of the same sign as the regional modelling results of Pelling and Green (2013) for 1, 2 and 5 m SLR cases with both fixed coastlines and coastal recession, however changes in the upper reaches of the Bay of Fundy were not replicated in
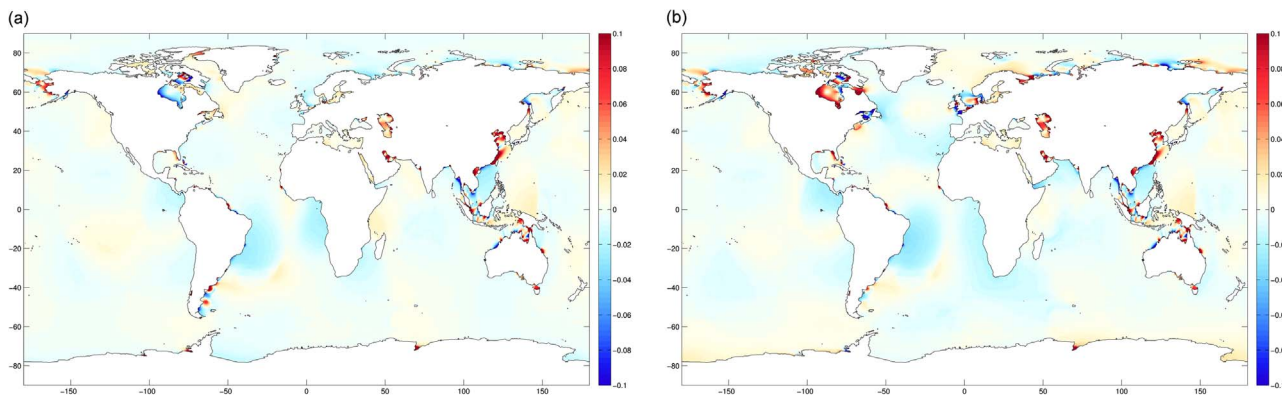

Fig. 6. a. Change in MHW (m) with an average of 2 m of non-uniform SLR from (a) Greenland (Fig. SM17) assuming a fixed coastline (+2NUGF) (b) Western Antarctica (Fig. SM18) assuming a fixed coastline (+2NUWAF) (increases- red, decreases- blue). For coastal city changes see Table 8.

the global model due to lower resolution. In addition to these model inter-comparisons some assessment of our model simulations of tidal changes with SLR in relation to those seen in observations can be found in the discussion of Mawdsley et al. (2015).

4.2. Implications of the changes

The principal implication of altered tidal amplitudes with SLR is for future coastal flood risk. With 1 m SLR, the high-end of the process based AR5 estimates for 2100 (Church et al., 2014), an increase or decrease in MHW ≥10 cm or ≤10 cm occurs at 13 of the coastal cities analysed with populations > 1 million in 2005. An increase or decrease of 10 cm may seem manageable, however, the relationship of return period and extreme water levels is log-linear; this means relatively small change in water level can cause a large change in the return period. A conservative estimate, particularly in tidally dominated regions (Haigh et al., 2010b), of the change in return period with SLR or tidal amplitude change is obtained by fitting a Gumbel distribution to the detrended annual maximum water levels. This simple assessment estimates that the MHW increases with 1 m SLR at Dhaka (13 cm), Ningbo (15 cm), Xiamen (7 cm) and New Orleans

(7 cm) would reduce the return period of the 1 in 100 yr water level to 1 in 60 yr, 1 in 60 yr, 1 in 63 yr and 1 in 73 yr events respectively. If the MHW increase and the SLR are taken into account the return period at all four cities decreases to less than a 1 in 2 yr event.

Currently national impact assessments such as the UKCP09 (Lowe et al., 2009) do not make an allowance for future tidal changes with SLR. However, results from this study, as well as Pickering et al. (2012) and other studies (de Ronde, 1986; Flather et al., 2001; Greenberg et al., 2012; Pelling and Green, 2013; Pelling et al., 2013b, 2013a), suggest an allowance for tidal changes should be included in coastal impact assessments for all countries. The Dutch Deltacommittee make a 10% allowance of the SLR imposed for the indirect effect of SLR on storm surges and any other effects (e.g. dredging and port alterations). For this to be sufficient the other factors and tidal change must not exceed 10% of the SLR. Our results show that changes > 10% of the SLR imposed are possible thus with the addition of the other effects the 10% allowance may be too small in places. Conversely, where SLR causes tidal decreases the 10% allowance may lead to over engineering of defences.

Any change in tidal elevation will affect tidal streams: a simple approximation (see Appendix A4) is that a 10% change in elevation

Table 8

Changes in MHW with a global average of 2 m SLR distributed non-uniformly according to initial elastic response sea-level fingerprints (Fig. 5, SM17 and SM18) associated with uniform melt of either the Greenland (+2NUGF), Western Antarctic (+2NUWAF) or Both (+2NUBF) of these two ice sheets. A scenario with melt from Both ice sheets that permits coastal recession with SLR (+2NUBR) is also included. MHW change values with 2 m uniform SLR for fixed (+2UF) and receding coastlines (+2UR) are provided for comparison. This subset of 40 of the 136 coastal cities with populations > 1 million is based the same criteria as Table 4.

COUNTRY, City/Agglomeration	Present Day Exposure Ranking		MHW (cm)						
	Population	Asset	Control	+2UF	+2NUGF	+2NUWAF	+2NUBF	+2UR	+2NUBR
ARGENTINA, Buenos Aires	64	52	98	−15	−17	−13	−15	−64	−63
AUSTRALIA, Adelaide	123	103	86	0	2	3	2	17	4
BANGLADESH, Chittagong	39	72	147	16	18	16	17	−13	−17
BANGLADESH, Dhaka	14	43	134	25	28	26	27	−1	−40
BANGLADESH, Khulna	23	54	87	−4	−4	−4	−4	19	16
BRAZIL, Belém	72	79	233	28	27	29	28	−131	−140
BRAZIL, Porto Alegre	78	83	14	7	7	6	7	18	19
CAMEROON, Douala	110	128	70	−3	−3	−2	−3	−16	−16
CANADA, Montréal	84	55	182	−8	8	−18	1	66	74
CHINA, Dalian	55	63	67	12	14	12	13	−3	−5
CHINA, Fuzhou Fujian	42	48	234	22	26	22	24	6	−1
CHINA, Guangzhou Guangdong	2	11	121	−23	−26	−24	−25	−19	−18
CHINA, Shenzen	18	31	100	−11	−14	−12	−13	−8	−7
CHINA, Hangzhou	92	108	166	16	19	17	18	25	19
CHINA, Ningbo	34	40	68	28	32	29	31	20	17
CHINA, Shanghai	3	13	205	−21	−23	−22	−23	−22	−19
CHINA, Taipei	49	59	85	16	19	17	18	8	5
CHINA, Tianjin	12	25	67	12	13	12	13	1	−3
CHINA, Xiamen	36	44	212	15	19	16	17	2	19
CHINA, Zhanjiang	40	45	112	−12	−13	−12	−13	−7	−6
NORTH KOREA, Namp'o	87	121	167	12	14	12	13	−6	−6
DENMARK, Copenhagen	82	53	27	9	4	8	17	15	−4
ECUADOR, Guayaquil	26	41	152	7	7	7	7	−71	−70
GERMANY, Hamburg	37	18	156	−1	−1	0	3	−96	−99
GUINEA, Conakry	70	113	156	−21	−19	−23	−22	−15	−16
INDIA, Calcutta	6	22	127	−12	−12	−11	−12	−43	−40
INDIA, Surat	24	46	228	9	14	7	11	26	22
INDONESIA, Palembang	48	73	76	18	19	20	19	−10	−21
INDONESIA, Surabaya	68	88	194	−25	−27	−29	−29	−50	−50
IRELAND, Dublin	95	62	129	12	−2	14	6	−22	−28
JAPAN, Hiroshima	44	24	175	−10	−11	−11	−11	−58	−68
MALAYSIA, Kuala Lumpur	35	33	127	6	7	7	7	−15	−20
MYANMAR, Rangoon	22	60	158	33	36	34	35	−6	−2
NETHERLANDS, Amsterdam	15	6	76	7	4	7	6	−33	−41
NETHERLANDS, Rotterdam	17	7	131	−8	2	−9	−4	−69	−75
SOUTH KOREA, Inchon	43	30	353	13	15	13	14	−10	−6
UNITED KINGDOM, Glasgow	91	68	133	5	0	6	2	−29	−36
USA, Houston	67	36	65	−15	−15	−13	−15	−30	−34
USA, New Orleans	10	3	16	14	11	16	14	16	17
VIETNAM, Ho Chi Minh City	5	27	128	−27	−30	−30	−30	−46	−57

amplitude would result in a 3% change in current amplitude. The results for maximum range changes at sites viable for new renewable energy extraction are therefore also indicative of associated changes in currents which are of direct importance for energy extraction. The potential alteration of the amount of available tidal energy with SLR must be taken into account when assessing future tidal energy resources. These alterations would affect cost-benefit analyses for tidal installations which typically have operational lifetimes of 25–120 years. Changes in the tidal currents will also have implications for the positions and intensity of tidal mixing fronts (e.g. Souza, 2013).

Tidal changes have implications for shipping; with increased range, lower low waters present a grounding risk (although this may be partially offset by the SLR itself). An additional difficulty is associated with higher high waters as tall ships may not be able to clear low bridges at high water when they have sufficient depth clearance below. Tidal changes in the Northwest Passages and Arctic Ocean also hold implications for shipping on newly opened routes arising due to ice melt.

Another possible feedback of tidal changes is on the rate of ice-calving in polar regions. An increased tidal range, such as the strong isolated MHW increases along the coast of Antarctica, might lead to an increased rate of ice-calving and hence SLR creating a positive feedback mechanism. The strong effect (~20%) of the spring-neap tide on the outflow of a key Antarctic ice stream has already been reported (Gudmundsson, 2006); changes to tidal characteristics could therefore plausibly be expected to influence the outflow of these streams which is pivotal in the rate of mass transport off the ice-sheets. Changing tides may also influence rates of sub glacial melting, see Mueller et al. (2012) and Sayag and Worster (2013).

4.3. Limitations of the study

Our approach to representing coastal recession with SLR was based on changing the model domain and admitting new wet cells. Owing to the 1 m vertical resolution of the bathymetric and topographic GEBCO dataset we are only able to investigate the effect of recession at SLR scenarios greater than 1 m. As the effect of recession on the tidal changes is shown to be significant at 2 m SLR it would be of interest to investigate this for 0.5 m and 1 m SLR scenarios. This would require a dataset with higher vertical resolution (at least around MSL) and a tidal model with higher horizontal resolution allowing more subtle (and more realistic) alterations in the coastline particularly around estuaries and barrier islands. Neither does this study take account of direct anthropogenic influence on the position of the coastline. Presently this is particularly relevant along the Chinese coast where large scale land reclamation of tidal flats is taking place. Studies on this effect for the East China Seas show there to be both localised changes to tidal characteristics as well as far field effects on Korean coast tide (Song et al., 2013); and for the Bohai Sea show increased tidal sensitivity to SLR (Pelling et al., 2013b). Coastline changes not associated with SLR in these regions may have equal (or greater) importance to (than) SLR on the tidal response.

Our model resolution of ~14 km limits the accuracy of coastline geometry in the vicinity of coastal cities, so further studies with unstructured grid models (e.g. Kernkamp et al., 2011) would be beneficial. A list of the cities located high up estuaries where the nearest representative coastal cell was taken is given in the SM Tables. For such locations (9 of 136) results should be interpreted with caution
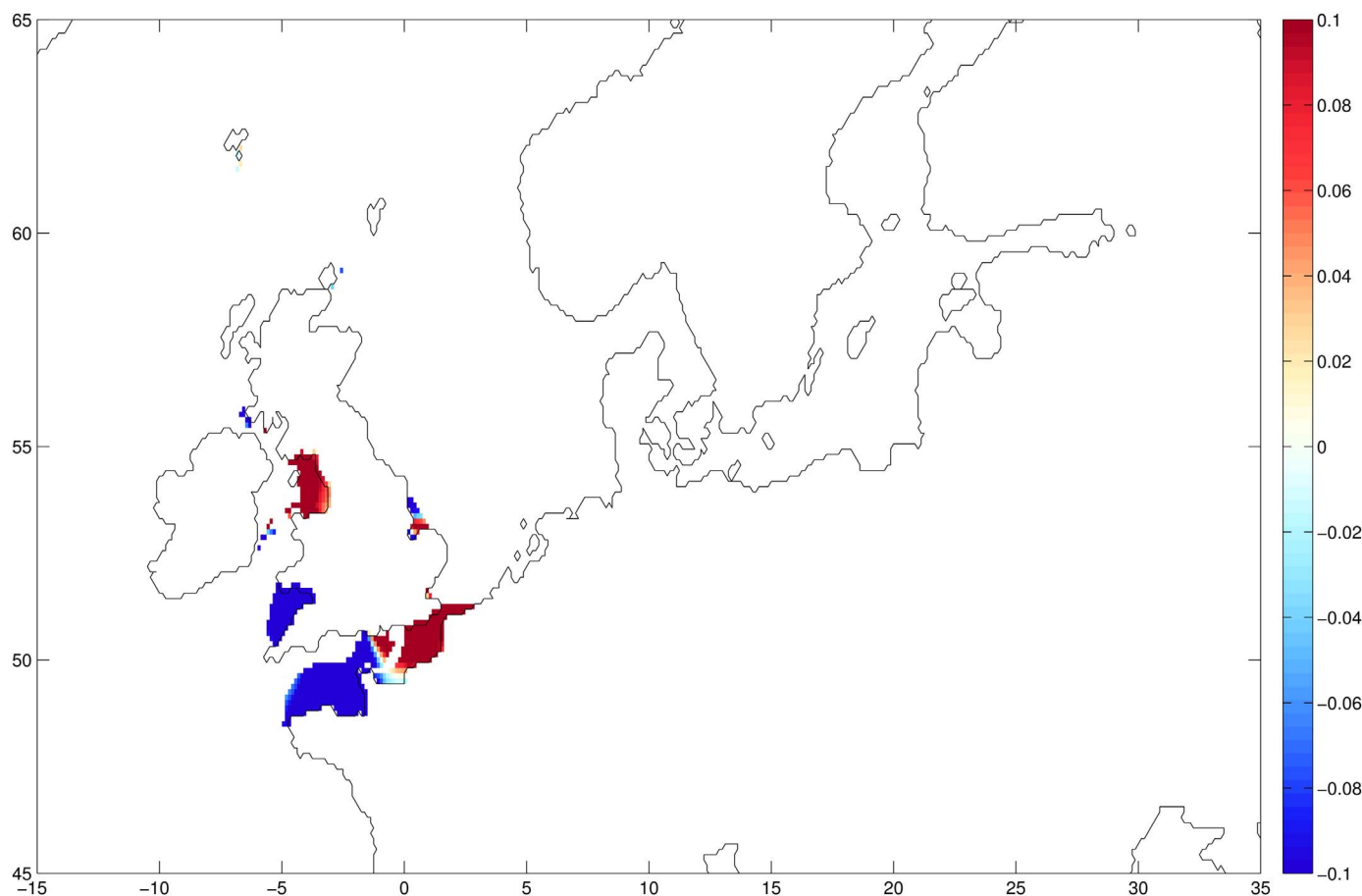

Fig. 7. European change in maximum range (m), over the 15 day SSH reconstruction based on the four tidal constituents, with a 2 m uniform SLR assuming a fixed coastline (+2UF) (increases- red, decreases- blue) for those locations found to be presently viable for tidal renewable energy (either 25–100 m depth and peak current velocities > 2 m/s or with a MTR > 5 m).

as potential differences between coastal projections and actual change at the city may occur. Whilst a barotropic approach to global tidal simulation is correct to first order, it is known that ocean stratification affects internal wave drag and can modulate tidal amplitude (Egbert et al., 2004). Furthermore Müller (2012) finds that a 10 m change in the mixed layer depth leads to a 1–2% change in tidal transports. Investigation of alterations to the tide with potentially increased future stratification due to climate change would be worthwhile further work.

The harmonic analysis used here only includes the primary tidal constituents M2, S2, K1 and O1; although higher harmonic tides will be generated within the model at this resolution they are not analysed. It has been shown (Pickering et al., 2012; Ward et al., 2012; Arns et al., 2015) that changes in higher harmonics on, for example, the European Shelf with SLR are non-negligible. It is a limitation therefore that the reconstruction on which the MHW is based does not include higher harmonics.

Finally, there are assumptions inherent in the IER sea-level fingerprints predictions (e.g. mass loss being uniform across the ice-sheet). Mitrovica et al. (2011) show the sensitivity of the fingerprints to this assumption to be limited to the near field. Additionally the sea-level fingerprints do not include the effect of the long-term viscous flow in the mantle or the steric sea-level effects of the ice mass loss. All SLR scenarios presented here do not include vertical land movement. This has to be incorporated subsequently for making engineering decisions, as is also the case for regional SLR projections (Katsman et al., 2011) and is performed for UKCP09 projections (Lowe et al., 2009).

5. Conclusions

This paper investigates the effect of future sea-level rise (SLR) on the global tides. We employed a global tidal model (Egbert et al., 2004), making refinements to the model setup to achieve improved representation of the present day tides and ensuring an appropriate physical setup for the future SLR perturbations. Various SLR scenarios are imposed including uniform and non-uniform patterns due to initial elastic response (IER) as well as comparing cases with fixed coastlines and permitting coastal recession. The main conclusions are as follows:

1) The tides in shelf seas across the globe change with SLR, with substantial localised tidal responses to plausible projections of SLR. The responses are significant on the east coast of the Americas, northwest Europe, north coast of Russia, across Asia and Australasia.
2) The tidal response is complex and exhibits spatially coherent increases and decreases in tidal amplitude.
3) Significant changes in the semidiurnal constituents (M2 and S2) with SLR occur in most shelf seas globally, whereas large changes in the diurnal tidal response (K1 and O1) are limited to seas around Asia.
4) The changes in semidiurnal constituents are often of the same sign (and will thus be additive during spring tides), but can also show opposing responses. This phenomena is explained in terms of the natural oscillation period of individual channels and basins.
5) The difference in the effect on the tidal response between including coastal recession with SLR versus assuming a fixed coastline is substantial. Permitting coastal recession amplifies the tidal response. However, more of the substantial changes become amplitude decreases in the recession case. New tidal areas due to coastal recession will however have flood risk implications.
6) The response of the tidal constituents, mean high water (MHW) and maximum range is shown to be non-proportional to the SLR imposed in many areas. With higher SLR a tendency towards above proportional MHW response is shown, suggesting a magnification of the tidal response at higher SLR (Table 6).
7) The inclusion of non-uniform SLR due to IER has a modest effect on the tidal response when compared with the uniform scenarios.

The tidal response is most dependent on the IER scenario at high latitudes where it is amplified in the far field and diminished in the near field of the ice-mass loss in the Greenland and Western Antarctic melt scenarios. Within 30 degrees of the equator all IER scenarios tend to amplify the tidal response owing to the above average SLR in the fingerprint. At Asian cities, the effect of all three IER scenarios is only to exacerbate the tidal response in addition to causing above average SLR. The influence of permitting coastal recession and IER results in greater differences with the uniform scenario than for the fixed coastline case.
8) The analysis at 136 largest coastal cities predicts MHW changes exceeding ± 10% of the SLR imposed at 13, 13 and 10 cities with +0.5UF, +1UF and +2UF respectively and at 18 cities with +2UR. Maximum range changes > 40 cm or < −40 cm with +2UF occur at 21 cities.

Projections of relative SLR for coastal management purposes consider global, and regional sea-level components (Slangen et al., 2014) as well as vertical land movements (Nicholls et al., 2014). This paper suggests that the patterns of MHW changes presented here should also be considered in these analyses and that national adaptation approaches to sea-level change should not assume tidal changes to be negligible. Given the importance of non-uniform SLR patterns for tidal changes shown in our results, future assessments of tidal changes should look to include additional components of regional sea-level rise (as well as IER) in the depth perturbations. Understanding tidal changes for the 0.5 m and 1 m SLR scenarios presented here, comparable to the mid to high-end IPCC RCP scenarios for global SLR in 2100, is particularly relevant for strategic coastal management. For the larger SLR cases considered here, which may occur over longer time-scales, adaptive management approaches to the problem are probably more appropriate, including this factor as an additional uncertainty (e.g. Ranger et al., 2013).

The strong effect of coastal recession on the modelled tidal response suggests that coastal management practises could influence the sign of the change in the tide with SLR. In some locations allowing coastal recession or imposing large scale sea walls can lead to reduced tidal amplitude with SLR; this tidal change could partially offset the increased coastal flood risk with SLR. Although allowing coastal recession on large scales may be possible, it is recognised that feasibility of large scale sea walls is more likely dependent on coastal land use and financial viability. To properly assess coastal management strategies using combinations of fixed coastlines and allowing retreat, one must make explicit simulations (rather than taking results from one of the two coastline scenarios presented here). This could be further investigated at a range of scales linking these global results down to shoreline management scales (Nicholls et al., 2013).

From an alternate perspective, that of the marine renewable energy planner, tidal amplitude (and current) increases are beneficial and decreases potentially problematic. It is suggested that when planning tidal renewable energy projects with long intended lifetimes, such as 120 years for the Severn barrage scheme, the potential future alteration to the tide by SLR should be considered, as the site may become more or less productive in the future. For further discussion of the implications of tidal changes with SLR see Pickering (2014).

Finally, given the substantial research effort into future SLR and its impacts, we suggest that further studies refining predictions of future tidal changes would be worthwhile. The global results presented here could be used as boundary conditions for very high resolution regional tidal models and as computational power increases higher resolution global simulations will also become possible.

Appendix A

A.1. Summary of online supplementary material

A) Animation of SSH (Eq. (3)) of present day tides: (i) 3 day and (ii) 15 day versions (.avi compatible with WM12+/VLC players)

B) A spreadsheet including: (a) full tables of all 136 largest coastal city results (extensions of Tables 4, 5, 8), (b) Tables SM1, SM2 and SM3 and their full versions (c) table of the latitude, longitude position of the model grid points used to represent the cities and flags for city centres far from this grid point (e.g. up an estuary) and the UHSLC tide gauge stations used for the return periods analysis, and (d) cumulative frequency distributions of the MHW changes at all 136 cities comparing all UF scenarios, and +2UF and +2UR scenarios (all changes normalised to 1 m SLR).

C) Figures relating to MHW methodological development. Figs. SM1−3d.

D) Regional enlargements of MHW changes with a 2 m uniform SLR with a fixed coastline (as in Fig. 3) and with coastal recession. Also maximum range change over the 15 day SSH reconstruction with 2 m uniform SLR and a fixed coastline. Figs. SM4a-10.

E) Regional proportionality plots (as in Fig. 4) with 1 m and 5 m uniform SLR and a fixed wall. Also MHW change in the 2 m SLF scenario to assess symmetry of tidal response about MSL. Figs. SM11a-16.

F) IER non-uniform SLR fingerprints for Greenland and Western Antarctic melt scenarios. Also MHW change in the combined fingerprint scenario both with a fixed coastline and permitting recession. Figs. SM17-19b.

G) Changes in the bottom energy dissipation with 2 m uniform SLR both with a fixed coastline and permitting recession. Figs. SM20a-20b.

H) Tidal changes plotted regionally with colour scales allowing comparison with other studies as outlined in Section 4.1. Figs. SM21−27f.

I) MHW changes as a percentage of the control amplitude for 1 m, 2 m and 5 m uniform SLR scenarios with a fixed coastline. Figs. SM28-30.

J) High resolution versions of figures from main text and supplementary material

A.2. Explanation of variations in SLR in coastal recession scenarios

In the recession cases lower SLR and occasional sea-level fall (SLF) values (e.g. Table SM1) are caused by the SLR perturbation applied to the GEBCO dataset (before the land masking is performed) bringing new, shallow, depth values into the average (up to 56 GEBCO points). Only values below mean sea-level are included in the average so with, for example, 2 m SLR the average would now include a number of new 1 m depth values (previously 1 m high land). Depending on the number of new shallow points the effect on the average is either to cause less SLR than intended or a SLF. The other factor that can lead to less than the intended SLR at the coast in the recession scenarios is the 2 m minimum depth applied to the bathymetry after the perturbation. For example if the control model cell average depth is 1 m it will be reset to 2 m, when 2 m SLR is applied to the control depth it will be 3 m leading to an actual imposition of only 1 m SLR rather than the 2 m in this scenario. These limitations only occur very close to the coast, the SLR imposed over the vast majority of the model domain is the intended value.

A.3. MHW method development explanation

Initially a MHW method was developed that takes the average of all peaks over a 15 day sea-surface height (SSH) reconstruction based on the four tidal constituents (Eq. (3)). The limitation of this method is that wherever a peak exists on the tidal curve, even short lived secondary maxima close to LW, they are erroneously taken into the average. This leads to unphysical spiral patterns in the MHW field often in the vicinity of tidal amphidromes. The second MHW method was to use the form factor (ff), see Eq. (A1), in order to determine whether to take the single highest maximum (diurnal regions $ff < 1.5$) or two highest maxima (semidiurnal regions $ff > 1.5$) per tidal day and then take the average of these.

$$ff_i = \left(\frac{Hm_{iK1} + Hm_{iO1}}{Hm_{iM2} + Hm_{iS2}} \right)$$

(A1)

where the ff is the ratio of the sum of the amplitudes of the diurnal constituents to the sum of the semidiurnal constituents. This has the advantage of omitting low secondary peaks in the tidal curve from the mean but the limitation, as shown in Fig. SM1, of introducing sharp unphysical MHW transitions in mixed tidal regions where the ff value goes from diurnal to semidiurnal and the number of maxima per tidal day changes. The solution to this, shown in Fig. SM2, was to identify an optimal percentile of the ranked SSH time series to represent MHW globally. Using the MHW from the ff method the optimum local percentile for each point was found and a global mean taken, giving the 88.8th percentile. To spatially smooth the field slightly the mean of a range (+/- 1 percentile) about the 88.8th percentile was taken. Some example points where the optimum local percentile is > 2 standard deviations of the global percentile field from the optimum mean global percentile are shown in Figs. SM3a-d. Locations where the ff MHW includes particularly low (high) peaks can be seen in Figs. SM3a-c (Fig. SM3d). A similar method was used to identify the optimum percentile for mean low water, found to be the 10.8 percentile. Further work looking to calculate MHWS and MHWN, also using peak based estimates to obtain a global percentile, found the 15 day maximum HW and the 71.3rd percentile to be the most representative values respectively.

A.4. Relationship of tidal amplitude and current changes

In many regions where tidal streams represent a viable energy resource (e.g. Pentland Firth, Menai Strait) the tidal currents are strong and rectilinear. Over the scale of interest there is no significant horizontal gradient of current, so the one-dimensional momentum equation reduces to a balance between the horizontal elevation gradient and bed friction, which is normally expressed as a quadratic parameterisation (e.g. $g.dz/dx = Cd\ U\ |U|/H$). If one considers the sea surface slope over some constant distance, dx, then this simplification leads to an expression where depth-averaged currents will change as the square root of the sea surface slope (i.e. $\Delta U = C\sqrt{(\Delta dz/dx)}$). One arrives at exactly the same relationship if considering open channel flow as favoured by engineers. Manning's equation (1891) expresses the depth-averaged velocity as proportional to the square root of the hydraulic slope. It follows that any change in tidal elevation will affect tidal streams in this way, and – as a simple approximation – a 10% change in elevation amplitude would result in a 3% change in current amplitude. The results for maximum range changes at sites viable for new renewable energy extraction are therefore also indicative of associated changes in currents which are of direct importance for energy extraction. The potential alteration of the amount of available tidal energy with SLR must be taken into account when assessing future tidal energy resources. These alterations would affect cost-benefit analyses for tidal installations which typically have operational lifetimes of 25–120 years.

Appendix B. Supporting information

Supplementary data associated with this article can be found in the online version at http://dx.doi.org/10.1016/j.csr.2017.02.004.

References

Arbic, B.K., Karsten, R.H., Garrett, C., 2009. On tidal resonance in the global ocean and the back-effect of coastal tides upon open-ocean tides. Atmos.-Ocean 47, 239–266.

Arns, A., Wahl, T., Dangendorf, S., Jensen, J., 2015. The impact of sea level rise on storm surge water levels in the northern part of the German Bight. Coast. Eng. 96, 118–131.

Austin, R.M., 1991. Modelling Holocene tides on the NW European continental shelf. Terra Nova 3, 276–288.

Caires, S., Diermanse, F., Dillingh, D., de Graaff, R., 2007. Extreme still water levels. In: Proceedings of the 10th International. workshop on wave hindcasting and forecasting and Coastal Hazard Symposium, WMO/TD-No. 1442, Hawaii, U.S.A, 11-16 November 2007.

Church, J., White, N., 2011. Sea-level rise from the late 19th to the early 21st century. Surv. Geophys. 32, 585–602.

Church, J.A., Clark, P.U., Cazenave, A., Gregory, J.M., Jevrejeva, S., Levermann, A., Merrifield, M.A., Milne, G.A., Nerem, R.S., Nunn, P.D., Payne, A.J., Pfeffer, W.T., Stammer, D., Unnikrishnan, A.S., 2014. Sea level change. In: Stocker, T.F., Qin, D., Plattner, G.-K., Tignor, M., Allen, S.K., Boschung, J., Nauels, A., Xia, Y., Bex, V., Midgley, P.M. (Eds.), Climate Change 2013: The Physical Science Basis. Working Group I Contribution to the Fifth Assessment Report of the Intergovernmental Panel on Climate Change. Cambridge University Press, Cambridge, United Kingdom and New York, NY, USA.

Dillingh, D., 2006. Waterstanden Nederlandse kust en estuaria- Statistieken t.b.v. de hydraulische randvoorwaarden, rapport RIKZ/2006.012, Den Haag, June 2006, Rijkswaterstaat RIKZ.

Egbert, G.D., Ray, R.D., 2000. Significant dissipation of tidal energy in the deep ocean inferred from satellite altimeter data. Nature 405, 775–778.

Egbert, G.D., Ray, R.D., 2001. Estimates of M-2 tidal energy dissipation from TOPEX/Poseidon altimeter data. J. Geophys. Res.-Oceans 106, 22475–22502.

Egbert, G.D., Ray, R.D., Bills, B.G., 2004. Numerical modeling of the global semidiurnal tide in the present day and in the last glacial maximum. J. Geophys. Res.-Oceans 109.

Flather, R.A., Baker, T., Woodworth, P., Vassie, I., Blackman, D., 2001. Integrated effects of climate change on coastal extreme sea levels. Proudman Oceanogr. Lab. Intern. Doc. No. 140, 20.

Flick, R.E., Murray, J.F., Ewing, L.C., 2003. Trends in United States tidal datum statistics and tide range. J. Waterw. Port Coast. Ocean Eng.-ASCE 129, 155–164.

Gebraad, A.W., Philippart, M.E., 1998. The Dutch Continental Shelf Model DCSM98: calibration using altimeter data, Werkdocument, RIKZ/OS-98.121x.

Gerritsen, H., Berentsen, C.W.J., 1998. A modelling study of tidally induced equilibrium sand balances in the North Sea during the Holocene. Cont. Shelf Res. 18, 151, (-+).

Green, J., 2010. Ocean tides and resonance. Ocean Dyn. 60, 1243–1253.

Greenberg, D.A., Blanchard, W., Smith, B., Barrow, E., 2012. Climate change, mean sea level and high tides in the Bay of Fundy. Atmos.-Ocean, 1–16.

Griffiths, S.D., Peltier, W.R., 2009. Modeling of polar ocean tides at the last glacial maximum: amplification, sensitivity, and climatological implications. J. Clim. 22, 2905–2924.

Grinsted, A., Moore, J.C., Jevrejeva, S., 2010. Reconstructing sea level from paleo and projected temperatures 200 to 2100 ad. Clim. Dyn. 34, 461–472.

Gudmundsson, G.H., 2006. Fortnightly variations in the flow velocity of Rutford Ice Stream, West Antarctica. Nature 444, 1063–1064.

Haigh, I., Nicholls, R., Wells, N., 2010a. Assessing changes in extreme sea levels: application to the English Channel, 1900–2006. Cont. Shelf Res. 30, 1042–1055.

Haigh, I.D., Nicholls, R., Wells, N., 2010b. A comparison of the main methods for estimating probabilities of extreme still water levels. Coast. Eng. 57, 838–849.

Hallegatte, S., Green, C., Nicholls, R.J., Corfee-Morlot, J., 2013. Future flood losses in major coastal cities. Nat. Clim. Change 3, 802–806.

Hanson, S., Nicholls, R., Ranger, N., Hallegatte, S., Corfee-Morlot, J., Herweijer, C., Chateau, J., 2011. A global ranking of port cities with high exposure to climate

extremes. Clim. Change 104, 89–111.

Hollebrandse, F.A.P., 2005. Temporal development of the tidal range in the southern North Sea (Master Thesis). Faculty of Civil Engineering and Geosciences, Delft University of Technology.

Jay, D.A., 2009. Evolution of tidal amplitudes in the eastern Pacific Ocean. Geophys. Res. Lett. 36.

Jevrejeva, S., Moore, J.C., Grinsted, A., 2012. Sea level projections to AD2500 with a new generation of climate change scenarios. Glob. Planet. Change 80–81, 14–20.

Jevrejeva, S., Grinsted, A., Moore, J.C., 2014. Upper limit for sea level projections by 2100. Environ. Res. Lett. 9, 104008.

Katsman, C., Sterl, A., Beersma, J.J., Brink, H.W., Church, J.A., Hazeleger, W., Kopp, R.E., Kroon, D., Kwadijk, J., Lammersen, R., Lowe, J., Oppenheimer, M., Plag, H.P., Ridley, J., Storch, H., Vaughan, D.G., Vellinga, P., Vermeersen, L.L.A., Wal, R.S.W., Weisse, R., 2011. Exploring high-end scenarios for local sea level rise to develop flood protection strategies for a low-lying delta—the Netherlands as an example. Clim. Change 109, 617–645.

Kernkamp, H.W.J., Van Dam, A., Stelling, G.S., de Goede, E.D., 2011. Efficient scheme for the shallow water equations on unstructured grids with application to the Continental Shelf. Ocean Dyn. 61, 1175–1188.

Lowe, J.A., Gregory, J.M., Flather, R.A., 2001. Changes in the occurrence of storm surges around the United Kingdom under a future climate scenario using a dynamic storm surge model driven by the Hadley Centre climate models. Clim. Dyn. 18, 179–188.

Lowe, J.A., Howard, T.P., Pardaens, A., Tinker, J., Holt, J., Wakelin, S., Milne, G., Leake, J., Wolf, J., Horsburgh, K., Reeder, T., Jenkins, G., Ridley, J., Dye, S., Bradley, S., 2009. UK Climate Projections Science Report: Marine and Coastal Projections. Met Office Hadley Centre, Exeter, UK, (<)⟨http://ukclimateprojections.defra.gov.uk/images/stories/marine_pdfs/UKP09_Marine_report.pdf⟩.

Lyard, F., Lefevre, F., Letellier, T., Francis, O., 2006. Modelling the global ocean tides: modern insights from FES2004. Ocean Dyn. 56, 394–415.

Mawdsley, R.J., Haigh, I.D., Wells, N.C., 2015. Global secular changes in different tidal high water, low water and range levels. Earth's Future 3, 66–81.

Merian, J.R., 1828. Ueber die Bewegung tropfbarer Flüssigkeiten in Gefässen [On the motion of drippable liquids in containers] (thesis) (in German). Schweighauser, Basel.

Milne, G.A., Gehrels, W.R., Hughes, C.W., Tamisiea, M.E., 2009. Identifying the causes of sea-level change. Nat. Geosci. 2, 471–478.

Mitrovica, J.X., Tamisiea, M.E., Davis, J.L., Milne, G.A., 2001. Recent mass balance of polar ice sheets inferred from patterns of global sea-level change. Nature 409, 1026–1029.

Mitrovica, J.X., Gomez, N., Morrow, E., Hay, C., Latychev, K., Tamisiea, M.E., 2011. On the robustness of predictions of sea level fingerprints. Geophys. J. Int. 187, 729–742.

Mudersbach, C., Wahl, T., Haigh, I.D., Jensen, J., 2013. Trends in extreme high sea levels along the German North Sea coastline compared to regional mean sea level changes. Cont. Shelf Res. 65, 111–120.

Mueller, R.D., Padman, L., Dinniman, M.S., Erofeeva, S.Y., Fricker, H.A., King, M.A., 2012. Impact of tide-topography interactions on basal melting of Larsen C Ice Shelf, Antarctica. J. Geophys. Res.: Oceans 117, C05005.

Müller, M., 2011. Rapid change in semi-diurnal tides in the North Atlantic since 1980. Geophys. Res. Lett. 38, L11602.

Müller, M., 2012. The influence of changing stratification conditions on barotropic tidal transport and its implications for seasonal and secular changes of tides. Cont. Shelf Res. 47, 107–118.

Müller, M., Arbic, B.K., Mitrovica, J.X., 2011. Secular trends in ocean tides: observations and model results. J. Geophys. Res.: Oceans 116, C05013.

Nerem, R.S., National Center for Atmospheric Research Staff, 2016. (Eds). Last modified 19 January 2016. The Climate Data Guide: Global Mean Sea Level from TOPEX & Jason Altimetry. Retrieved from ⟨https://climatedataguide.ucar.edu/climate-data/global-mean-sea-level-topex-jason-altimetry⟩.

Nicholls, R.J., Hanson, S., Herweijer, C., Patmore, N., Hallegatte, S., Corfee-Morlot, J., Château, J., Muir-Wood, R., 2008. Ranking port cities with high exposure and vulnerability to climate extremes: exposure estimates. Paris, France, Organisation

for Economic and Co-operative development (OECD), 62pp. (Environment Directorate Working Papers, (ENV/WKP(2007)1)).

Nicholls, R.J., Townend, I.H., Bradbury, A.P., Ramsbottom, D., Day, S.A., 2013. Planning for long-term coastal change: experiences from England and Wales. Ocean Eng. 71, 3–16.

Nicholls, R.J., Hanson, S.E., Lowe, J.A., Warrick, R.A., Lu, X., Long, A.J., 2014. Sea-level scenarios for evaluating coastal impacts. Wiley Interdiscip. Rev.: Clim. Change 5, 129–150.

Passeri, D.L., Hagen, S.C., Plant, N.G., Bilskie, M.V., Medeiros, S.C., Alizad, K., 2016. Tidal hydrodynamics under future sea level rise and coastal morphology in the Northern Gulf of Mexico. Earth's Future 4, 159–176.

Pelling, H.E., Green, J.A.M., 2013. Sea level rise and tidal power plants in the Gulf of Maine. J. Geophys. Res.: Oceans 118, 2863–2873.

Pelling, H.E., Uehara, K., Green, J.A.M., 2013b. The impact of rapid coastline changes and sea level rise on the tides in the Bohai Sea, China. J. Geophys. Res.: Oceans 118, 3462–3472.

Pelling, H.E., Green, J.A.M., Ward, S.L., 2013a. Modelling tides and sea-level rise: to flood or not to flood. Ocean Model. 63, 21–29.

Pickering, M., 2014. The Impact of Future Sea-level Rise on the Tides. University of Southampton, UK, Ocean and Earth Science, 347.

Pickering, M.D., Wells, N.C., Horsburgh, K.J., Green, J.A.M., 2012. The impact of future sea-level rise on the European shelf tides. Cont. Shelf Res. 35, 1–15.

Platzman, G.W., Curtis, G.A., Hansen, K.S., Slater, R.D., 1981. Normal modes of the world ocean. Part II: description of modes in the period range 8 to 80 h. J. Phys. Oceanogr. 11, 579–603.

Pouvreau, N., Martin Miguez, B., Simon, B., Wöppelmann, G., 2006. Évolution de l'onde semi-diurne M2 de la marée à Brest de 1846 à 2005. Comptes Rendus Geosci. 338, 802–808.

Provost, C.L., 2001. Ocean tides. In: Fu, L.-L., Cazenave, A. (Eds.), Satellite Altimetry and Earth Sciences 69. Academic Press, London.

Pugh, D., 1987. Tides, surges and mean sea-level Chichester. John Wiley & Sons Ltd.

Pugh, D.T., 2004. Changing sea levels. Effects of tides, weather and climate. Cambridge University Press.

Pugh, D.T., Vassie, J.M., 1980. Applications of the joint probability method for extreme sea level computations. Proc. Inst. Civ. Eng. Part 2 69, 959–975.

Ranger, N., Reeder, T., Lowe, J., 2013. Addressing 'deep' uncertainty over long-term climate in major infrastructure projects: four innovations of the Thames Estuary 2100 Project. Eur. J. Decis. Process. 1, 233–262.

Ray, R.D., 2006. Secular changes of the M-2 tide in the Gulf of Maine. Cont. Shelf Res. 26, 422–427.

Ray, R.D., 2009. Secular changes in the solar semidiurnal tide of the western North Atlantic Ocean. Geophys. Res. Lett. 36.

de Ronde, J.G., 1986. Bepaling knoopfactoren harmonische analyse met het Continental Shelf Model, Notitie GWAO-86.309, Dienst Getijdewateren, Rijkswaterstaat.

Sayag, R., Worster, M.G., 2013. Elastic dynamics and tidal migration of grounding lines modify subglacial lubrication and melting. Geophys. Res. Lett. 40, 5877–5881.

Schwiderski, E.W., 1980. On charting global ocean tides. Rev. Geophys. 18, 243–268.

Slangen, A.B.A., Carson, M., Katsman, C.A., van de Wal, R.S.W., Kohl, A., Vermeersen, L.L.A., Stammer, D., 2014. Projecting twenty-first century regional sea-level changes. Clim. Change 124, 317–332.

Song, D., Wang, X.H., Zhu, X., Bao, X., 2013. Modeling studies of the far-field effects of tidal flat reclamation on tidal dynamics in the East China Seas. Estuar. Coast. Shelf Sci. 133, 147–160.

Souza, A.J., 2013. On the use of the Stokes number to explain frictional tidal dynamics and water column structure in shelf seas. Ocean Sci. 9, 391–398.

Sriver, R., Urban, N., Olson, R., Keller, K., 2012. Toward a physically plausible upper bound of sea-level rise projections. Clim. Change 115, 893–902.

Uehara, K., Scourse, J.D., Horsburgh, K.J., Lambeck, K., Purcell, A.P., 2006. Tidal evolution of the northwest European shelf seas from the Last Glacial Maximum to the present. J. Geophys. Res.: Oceans 111, C09025.

Ward, S., Green, J.A.M., Pelling, H., 2012. Tides, sea-level rise and tidal power extraction on the European shelf. Ocean Dyn. 62, 1153–1167.

Woodworth, P.L., 2010. A survey of recent changes in the main components of the ocean tide. Cont. Shelf Res. 30, 1680–1691.

Woodworth, P.L., Shaw, S.M., Blackman, D.L., 1991. Secular trends in mean tidal range around the British Isles and along the adjacent European coastline. Geophys. J. Int. 104, 593–609.

Zaron, E.D., Egbert, G.D., 2006. Estimating open-ocean barotropic tidal dissipation: the Hawaiian Ridge. J. Phys. Oceanogr. 36, 1019–1035.

Further reading

Manning, R., 1891. On the flow of water in open channels and pipes. Trans. Inst. Civ. Eng. Irel. 20, 161–207.